

Techniques for investigating the near-Earth space environment

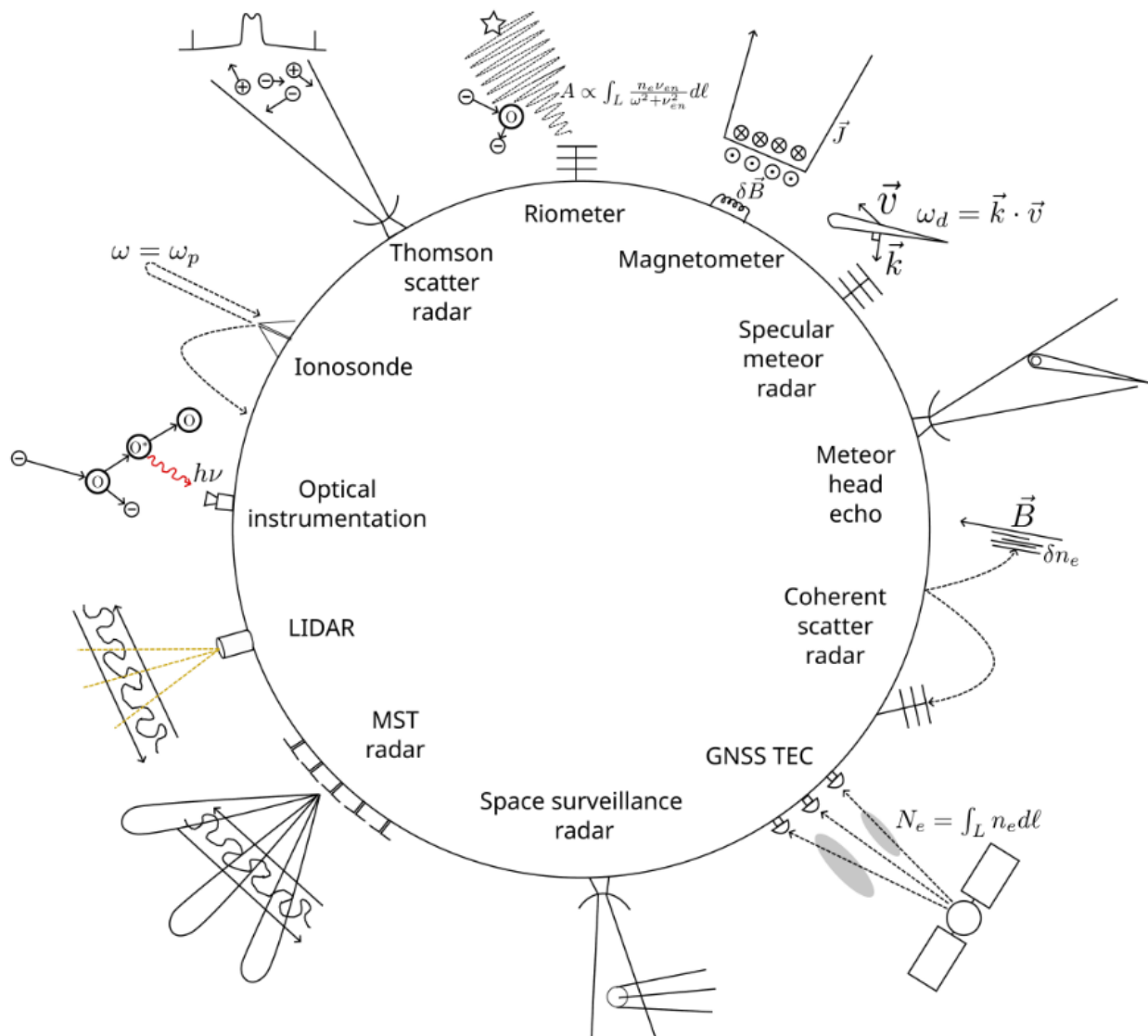
NoteBook

TRYM VARLAND

GitHub: tva050

UiT - Norges Arktiske Universitet

May 20, 2024



Acknowledgment

I would like to give a big thanks to Juha-Pekka Vierinen the course responsible, for all the lectures and the composite of the course which gave insight into different instruments that can be used for investigating the near-Earth Space environment.

Also thanks to Björn Gustavsson, Magnar Gullikstad Johnsen, Theresa Rexer, Devin Huyghebaert, Njål Gulbrandsen, and Andres Spicher as guest lecturers and for making The Heimdal campaign successful.

A last thank's to Etienne Robin Victor Gavazzi as the course assistant, and great seminars.

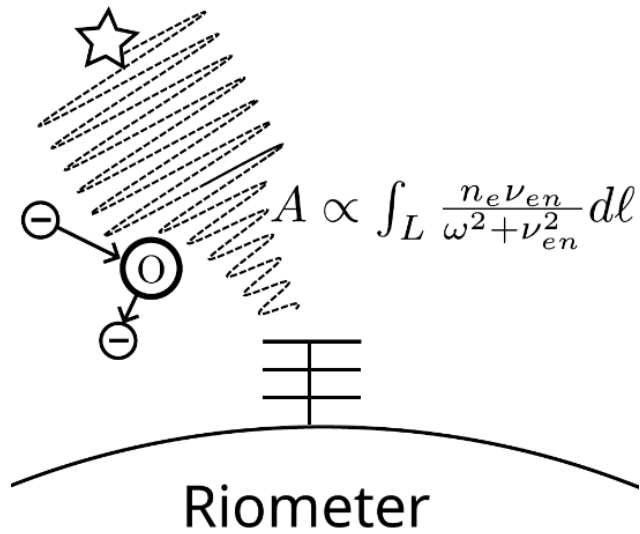
Contents

1 Riometer Exercise	4
1.1 Riometer description	4
1.2 Power as a function of time	4
1.3 Temperature brightness	5
1.4 Plasma frequency	5
1.5 The mistake	5
1.6 Multi-frequency and wide band riometer	7
1.7 Radio interference	7
1.8 Radio wave absorption	8
1.9 Attenuation and absorption	9
1.10 Absorption prog	9
2 Ionosonde Exercise.....	12
2.1 Ionosonde description.....	12
2.2 Ionogram F2-region.....	13
2.3 Reflection (ionogram copies)	13
2.4 O-mode and X-mode cutoff freq	14
2.5 Two circularly polarized electromagnetic waves	14
2.6 Automatically scaled foF2 correct?.....	15
2.7 foF2 parameter scaled wrong again.....	16
2.8 HF sounding of the ionosphere	17
2.9 electron density profile.....	17
2.9.1 foF2 parameter in an ionogram	17
2.9.2 O-mode wave propagating	18
2.9.3 O-model reflection altitude	19
2.9.4 Calculate the group velocity of the O-mode wave	20
2.10 O-mode trace simulated	22
3 Meteor radar Exercise.....	26
3.1 Feature of the measurement containing temperature.....	26
3.2 Meteor head echoes and strongest trail echo.....	26
3.3 factors contribute to the mass-loss of meteors	27
3.4 Very slow meteor.....	27

3.5	Hyperbolic orbit	28
3.6	Ionized meteor trail evolution	28
3.7	Sinusoidal oscillations and five different phases	29
3.8	Estimate the zonal and meridional winds	29
4	Total Electron Content (TEC)	32
4.1	Ionospheric contribution to measured distance (pseudorange).....	32
4.2	Errors in ionospheric delay - and TEC measurements	33
4.3	Vertical TEC and slant TEC	36
4.4	Errors in vertical TEC from slant TEC	37
4.5	Differential TEC	37
4.6	Line integral of electron density.....	38
4.7	Pseudorange and carrier phase for observing ionospheric TEC	39
4.8	Plotting the vertical TEC (St Patrick's Day Storm)	40
5	Magnetometer exercises	41
5.1	Generation mechanisms and typical magnetic flux densities.....	41
5.2	Fluxgate- and proton precision magnetometers	42
5.3	Magnetometer coordinates H, D, Z and I	42
5.4	challenges when measuring Earth's magnetic field.....	43
5.5	line current and is it westward or eastward?.....	44
5.6	Negative or positive disturbance, for Tromsø and Svalbard Magnetometers	45
6	Optical Observations	47
6.1	Keogram.....	47
6.2	Narrow band filters	48
6.3	Magnetic field look direction.....	48
6.3.1	Three wavelengths for auroral research	49
6.4	Interesting auroral event (Tromsø AI)	49
6.5	Calibrate the mapping	51
6.6	Calculating the unit vectors from two different auroral imagers.....	51
7	Incoherent scatter radar exercises.....	53
7.1	Primary plasma parameters	53
7.2	The attribute "collective"	54
7.3	Calculate the radar cross-section	54
7.4	Calculate the ratio of received echo power and system noise power	55
7.5	sketch the ion-line feature and explain the plasma parameters	56
7.6	Optimal incoherent scatter radar frequency and performance degrade.....	56
7.7	Three examples of other uses for these large radars	57
7.7.1	Planetary Radar Astronomy	57
7.7.2	Atmospheric dynamics and space weather	57
7.7.3	Ionospheric experiments	57
7.8	The magic constant γ	58

7.9	Range-time diagram to describe where in range-time space the radar scatter originates from	59
7.10	Plasma-parameters.....	60
7.11	Scattered power reduced proportionally to $1/R^2$	61
8	Meteor head echo exercises.....	62
8.1	Meteor head echo	62
8.2	Radar cross-section of a meteor head.....	63
8.3	Estimating meteoroid mass	63
8.4	Derive the Halliday equation and assumptions	64
8.5	Interferometry and tri-static observation of trajectory	65
8.6	Determine the velocity and acceleration of the meteor (MAARSY).....	65
9	Space debris exercises	68
9.1	Kessler syndrome	68
9.2	parameters to obtain information about the properties of the space debris objects	69
9.3	relate antenna gain G and antenna effective area A_{eff}	69
9.4	Diameter much smaller than the wavelength	70
9.5	Signal-to-noise ratio for a 0.1 m diameter cubesat.....	70
9.6	Furthest distance that you can observe the cubesat	71
10	Coherent scatter exercises.....	73
10.1	The SuperDARN over-the-horizon radar network observes the F-region (gradient drift instability mechanism)	73
10.1.1	Snell's law, ray paths of radio waves, Appleton-Hartree equation . . .	73
10.1.2	Typical radio wave ray path between the radar and the region of ionospheric scatter	74
10.1.3	radar Bragg wave vector, scattered signal	75
10.1.4	Information from the Doppler shift of F-region	75
10.2	range-time diagram, different time lags of the autocorrelation function, multi-pulse scheme	76
10.3	Northern Hemisphere polar cap convection patterns	77
10.3.1	solar wind magnetic field, convection pattern	77
10.3.2	ionospheric convection pattern, 2024-03-11T22:45	77
11	Appendix	78

1 Riometer Exercise



1.1 Riometer description

Explain in your own words, what is a riometer. Include reference to your favorite scientific article about riometers. Use less than 200 words.

The relative ionospheric opacity meter, also called the riometer is a radio receiver that is measuring cosmic radio noise. As the footprint of the riometer is small well as the energy needed and it averages over a larger region of the sky, it offers a routine ground-based method for measuring and monitoring the intensity of the cosmic radio noise. The riometer is measuring the amount of power that is on average received when no anomalous absorption is present, we say on average as also noise is received. It measures the amplitude of the signals received, in a band between 20 and 70MHz. At this band the ionosphere, is less disturbed. My favorite scientific article about riometers is the first one [1].

1.2 Power as a function of time

Riometers measure power as a function of time. In the absence of any sporadic ionospheric perturbations, measured power repeats with a certain period. What is this period measured in days?

As the riometer is measuring the cosmic radio noise absorption in the Earth's ionosphere, the ionospheric perturbations is related to the daily variation of Earth rotation. As Earth is rotating around it's axis, the riometer measurements experiences variations in the ionospheric conditions due to the change in the angle of the incident cosmic radio noise.

There for the period measured in days in the absence of sporadic ionospheric perturbations is approximately one day.

1.3 Temperature brightness

How much brighter is the Milky Way at 50 MHz compared to 200 MHz in terms of radio brightness temperature?

To calculate how much the brighter the Milky way is at 50MHz compared to 200MHz in terms of radio brightness temperature, we need to use the following power law equation.

$$T_{gal}(\nu) = T_{150} \left(\frac{\nu}{\nu_{150}} \right)^{-\beta} \quad (1)$$

Where $\beta = 2.5 \pm 0.1$ also called the *spectral index*. Than we can compare the two frequencies.

$$\frac{T_{50}}{T_{200}} = \frac{\left(\frac{50}{150}\right)^{-2.5}}{\left(\frac{200}{150}\right)^{-2.5}} = \underline{\underline{32}}$$

Hence the galactic brightness temperature at 50MHz is 32 time the brightness temperature at 200MHz.

1.4 Plasma frequency

Several figures in Ocker et.al., 20218 show measurements of Lang-muir waves by the Voyager 1 space probes plasma wave sensor. Use the formula for plasma-frequency to convert electron plasmafrequency to electron density in units of electrons per cubic meter. What is the approximate value between 2019-2020?

Now we gone convert the electron plasma frequency to electron density in units of electrons per cubic meter, where we use the approximation of the plasma frequency measured between 2019-2020 by the Voyager 1 space probes plasma wave sensors. This approximation is about 3kHz, so than we can re-formulate the plasma frequency expression.

$$\omega_p = \left(\frac{n_0 e^2}{\epsilon_0 m} \right)^{1/2} \quad \Rightarrow \quad n_0 = \frac{\omega_p^2 m \epsilon_0}{e^2} \quad (2)$$

Now we can compute with the known values, and we get.

$$n_0 = \frac{3000^2 \cdot 9.109 \times 10^{-31} \cdot 8.854 \times 10^{-12}}{1.602 \times 10^{-19}} \approx \underline{\underline{0.0584 m^{-3}}}$$

We will have 0.0584 electrons per cubic meter, in the period between 2019 and 2020.

1.5 The mistake

Many textbooks and scientific papers that show a Figure like the one shown below have a mistake. Can you figure out what is the mistake?

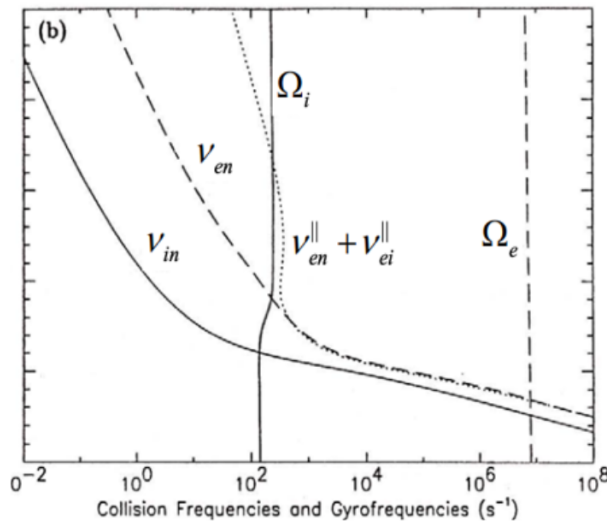


Figure 1: textbooks and scientific papers gyro-frequency error.

As we can see in the image given in the task 1, the x-axis is given in s^{-1} . If we compare the value of the electron gyro-frequency ω_e , with the following plot:

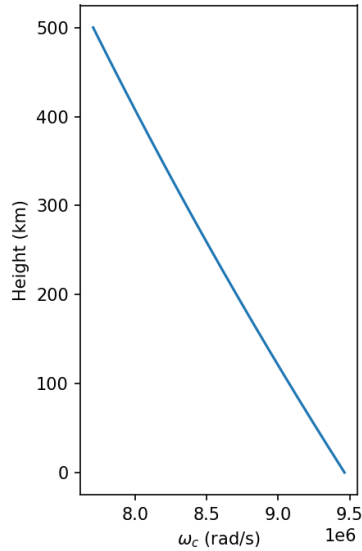


Figure 2: electron gyro-frequency between 0-500km

We see that the value of ω_e in the originally plot is given in the wrong factor and should be rad/s instead. This means that the ω_e will have a smaller value than represented in the task image shown at the top 1.

```

1 lat = 69.65
2 lon = 18.96

```

```

3 h = np.linspace(0,500,500) # 0 to 500 km
4 date = datetime(2024,1,17)
5 Be, Bn, Bu = ppigrf.igrf(lon,lat,h,date)
6
7 # Absolut value of B
8 B_abs=n.sqrt(Be[0,:]**2.0 + Bn[0,:]**2.0 + Bu[0,:]**2.0)/1e9
9 plt.plot(c.e*B_abs/c.electron_mass,h)
10 plt.xlabel("$\omega_c$ (rad/s)")
11 plt.ylabel("Height (km)")
12 plt.show()

```

Listing 1: Code for electron-frequency plot (Fig. 2)

1.6 Multi-frequency and wide band riometer

What advantages are there for using a multi-frequency or wide band riometer. Provide at least two advantages.

The **first advantages** of using multi-frequency or wide-band riometer, is that different frequencies is absorbed differently in the ionosphere, depending on the factors such as electron density, temperature and solar activity. By using multi-frequencies or a wide band system, a riometer can better discriminate between different ionospheric effects.

The **second advantage** is that multi-frequency or wide-band riometer, provide a broader range of information about the ionospheric conditions. As it more sensitive, and the measurements have less artifacts (etc. noise, radio interference).

1.7 Radio interference

Identify regions with radio interference in the measured absorption in the following Figure. Explain what in the measurement points to these regions being interference.

We are asked to find the radio artifacts in the measured absorption plot, and the following radio interference is found, marked with a red arrow.

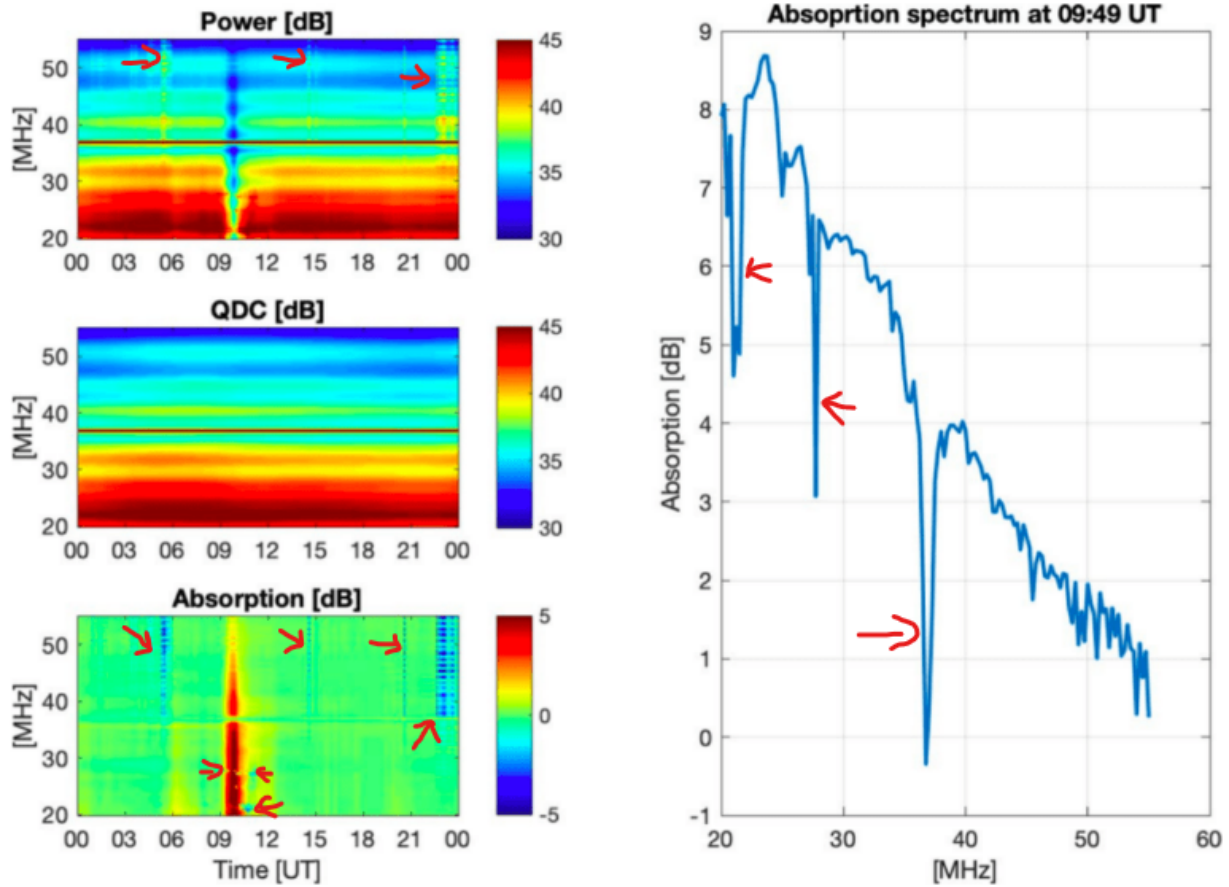


Figure 3: interference

We know that the radio interference, can cause false negative absorption measurements and for the color plots we get low powered horizontal lines in the plot.

1.8 Radio wave absorption

In which of the following telecommunications applications should you be worried about radio wave absorption due to electron-neutral collisions: a) GNSS positioning, b) GSM cell phone communications, c) HF telecommunications links that rely on ionospheric reflection. Explain why.

The **GNSS positioning** we are not that concerned about radio wave absorption due to electron-neutral collisions, as this type of signals operates in the L-band frequencies (1.2-1.5GHz).

For the **GSM cell phone communications**, we are a little bit concerned. As this signal is operating in the 900-1800MHz bands, they are not that effected of absorption due to electron-neutral collisions in the atmosphere. But in some weather conditions, we we can see the effect of this.

HF telecommunications links that rely on ionospheric reflection, we are highly concerned

about absorption's of radio waves due to electron-neutral collisions. As for high-frequency telecommunications link are operating in the 3-30MHz range and relays on the ionospheric reflection for long distance communications. In this frequency range, radio waves interacts significantly with the ionosphere, and absorption due to electron-neutral collisions becomes a critical factor.

1.9 Attenuation and absorption

A riometer measures an absorption of 6 dB at 30 MHz. How much attenuation does the cosmic radio noise experience (in linear units). Can you estimate how much absorption will occur at 60 MHz, assuming that $\omega \gg \nu_{en}$ and $\omega \gg \omega_c$. Here ω is the radio wave angular frequency, ν_{en} is the electron-neutral collision frequency, and $\omega_c = eB/m_e$ is the electron gyro-frequency.

For calculating the linear attenuation of cosmic radio noise, we use the formula.

$$\text{linear attenuation} = 10^{A/20} = 10^{6/20} \approx \underline{\underline{0.5}} \quad (3)$$

So the linear attenuation at 30MHz is $10^{6/20}$. Now for calculating the absorption at 60MHz, with the assumption that $\omega \gg \nu_{en}$ and $\omega \gg \omega_c$. We have the formula.

$$A(\nu) = A(\nu_0) + 20 \cdot \log_{10} \left(\frac{\nu}{\nu_0} \right) \quad (4)$$

Given that $A(\nu_0) = 6dB$ at 30MHz, we can estimate the absorption at 60MHz.

$$A(60MHz) = 6 + 20 \log_{10}(2) \approx \underline{\underline{12dB}}$$

So at 60MHz we have a absorption of 12dB.

1.10 Absorption prog

There is some code in https://github.com/jvierine/fys3002/blob/main/ex00/sim_riometer.py that evaluates an electron density profile based on a solution to the steady-state continuity equation

$$\frac{dn_e}{dt} = q - \alpha n_e^2 = 0 \quad (5)$$

You are provided with q , and recombination-rate α . The program also uses PyMIS to obtain a neutral density profile, and evaluates the electron-neutral collision-frequency based on the N_2 molecular density. Use the formula in e.g., Hargreaves (1969) to calculate the absorption of radio waves that propagate vertically through the ionosphere. Evaluate frequencies of $f = 10, 15, 30, 60, 120MHz$. Evaluate both extraordinary and ordinary mode absorption. Make a plot of absorption as a function of frequency for both modes. Which mode is absorbed more?

From the plot in figure 4, we see that the extraordinary mode (x-mode) has the most absorption at different frequencies that is calculated using formula from Hargreaves.

$$A_{dB} \approx 4.61 \cdot 10^{-5} \int \frac{n_e \nu_{en}}{(\omega \pm \omega_c)^2 + \nu_{en}^2} dx \quad (6)$$

This comes from the fact that different polarization have different propagation paths through the ionosphere. As we send a linearly polarized electro-magnetic wave in the vertical direction, the right-hand circular polarization (x-mode) will be first reflected. This makes sense since we can see that the x-mode has more absorption at different wavelengths than the o-mode.

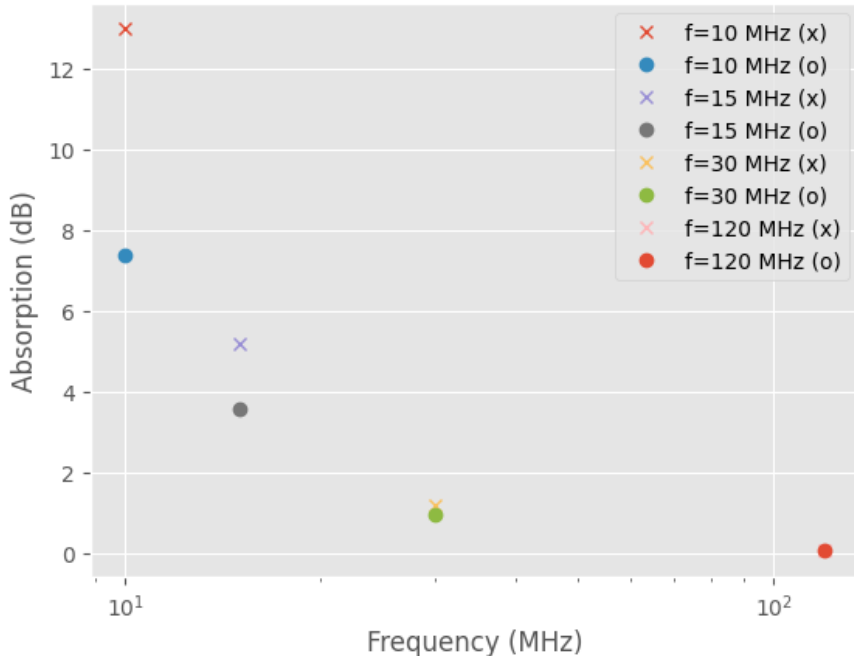


Figure 4: Absorption of radio waves that propagate vertically through the ionosphere. Here • (o) and x, is the ordinary- and extraordinary mode.

```

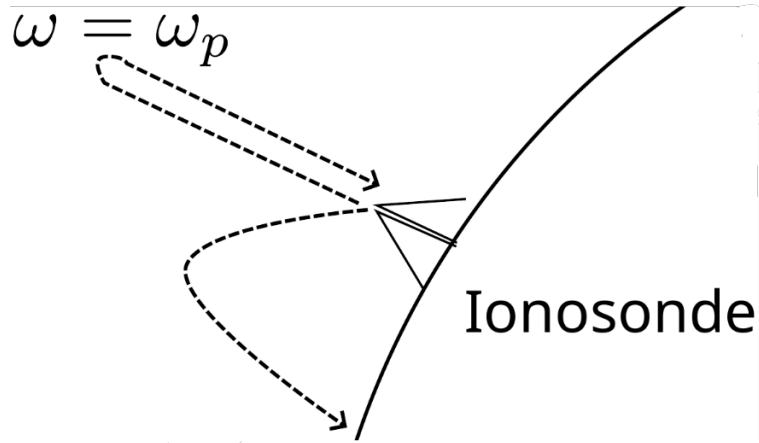
1 frequencies = [10e6, 15e6, 30e6, 120e6] # frequencies given
2 for i in frequencies:
3     omega = 2*n.pi*i
4     omega_c = 2*n.pi*1.4e6
5
6     absorption_x = n.trapz(4.6e-5*n_e*nu_en / (nu_en**2.0 + (omega - omega_c)**2.0), hgt, dx=dh)
7     absorption_o = n.trapz(4.6e-5*n_e*nu_en / (nu_en**2.0 + (omega + omega_c)**2.0), hgt, dx=dh)
8
9     plt.semilogx(i/1e6,absorption_x,"x",label="f=%1.0f MHz (X)"%(i/1e6))
10    plt.semilogx(i/1e6,absorption_o,"o",label="f=%1.0f MHz (O)"%(i/1e6))
11 plt.xlabel("Frequency [MHz]")
12 plt.ylabel("Absorption [dB]")

```

```
13 plt.legend()  
14 plt.show()
```

Listing 2: code for calculating the absorption of radio waves

2 Ionosonde Exercise



2.1 Ionosonde description

Explain in your own words, how an ionosonde works and what it measures. Include reference a scientific article or book that includes ionosonde measurements. Use less than 200 words.

An ionosonde is a device that measures the electron density in the Earth's ionosphere. It operates by transmitting a high-frequency radio signal vertically into the ionosphere. As the signal travels upward, it will encounter electrons in the ionosphere and courses reflection back to earth. So to get the overview picture of the ionosphere behavior, we need to measure all the parameters that is describing the reflected radio wave. These parameters are:

1. Group travel time
2. Amplitude
3. Phase
4. Doppler offset
5. incidence angle
6. wave polarization
7. Curvature of the wave front

With help of the mentioned parameters we are able to get a picture of the structure and the motion that we find in our ionosphere. All information, is retreated from [2] and [3].

2.2 Ionogram F2-region

Obtain a realtime ionogram from the Sodankylä Geophysical Observatory ionosonde: Save the image to your report. If you can see the foF2 feature in the ionogram, mark it and estimate the peak plasma density of the F2-region. Also estimate the h'F parameter, if you can see it.

In figure 5 we see a ionogram using O-mode, where we the vertical black line is showing the foF2 feature and the horizontal line is showing the h'F feature. By analysing the measurement we can see that the peak plasma density of the F2-region is at $\approx 9.4\text{MHz}$, so than we can calculate the density by using 2:

$$n_0 = \frac{\omega_p^2 m \epsilon_0}{e^2} = \frac{9.4 \times 10^6 \cdot 9.109 \times 10^{-31} \cdot 8.854 \times 10^{-12}}{1.602 \times 10^{-19}} \approx \underline{\underline{4.5 \times 10^8 \text{m}^2}}$$

Estimated peak plasma density of the F2-region today (27.01.2024) is about $4.5 \times 10^8 \text{m}^2$. By looking at the plot it looks reasonable that the virtual height is about $h'F \approx 202\text{km}$.

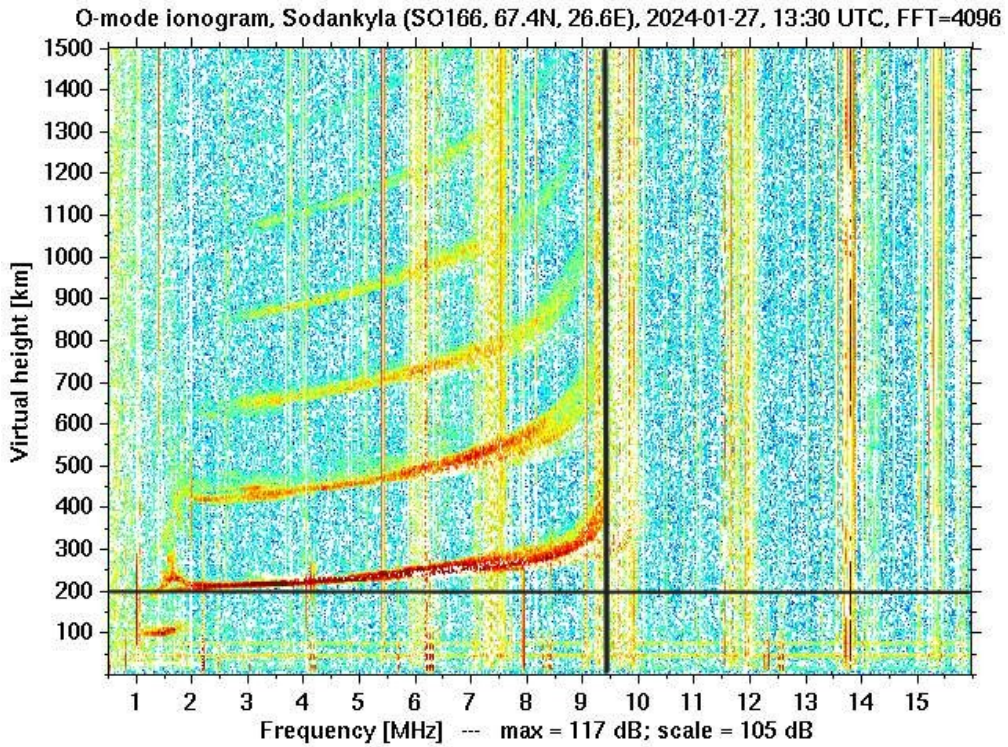


Figure 5: O-mode ionogram, Sodankyla 2024-01-17. foF2 and h'F marked.

2.3 Reflection (ionogram copies)

In the ionogram shown above, there appear multiple copies of the F-region trace. Explain why these appear.

As seen in figure 5, we have multiple copies of the F-region trace. These appears when we have multiple bounces of the radio wave between the ground and the ionosphere, which happens when a matvhing condition between electron density and radio wave frequency is met.

2.4 O-mode and X-mode cutoff freq

Calculate the expected separation between the O-mode and Xmode cutoff frequencies above Tromsø, assuming that the cold plasma resonance frequency is 5 MHz and the electron gyro-frequency is 1.3 MHz.

We have that the cold plasma resonance frequency (ω_p) is 5MHz and the electron gyro-frequency (ω_c) is 1.3MHz. For calculating the expected separation between the O-mode and X-mode cutoff frequencies above Tromsø, we can subtract them from each other. We are first going to calculate the O-mode peak, where the following expression is used.

$$\begin{aligned}\omega_O &= \omega_p = \sqrt{\frac{e^2 n_e}{\epsilon_0 m_e}} \\ &= \underline{5.0 \times 10^6 \text{ Hz}}\end{aligned}\tag{7}$$

Than calculating the X-mode.

$$\begin{aligned}\omega_X &= \frac{1}{2}[\omega_c + (\omega_c^2 + 4\omega_p^2)^{1/2}] \\ &= \frac{1}{2}[1.3 \times 10^6(1.3 \times 10^{12} + 4 \cdot 5 \times 10^{12})^{1/2}] \\ &\approx \underline{2.956 \times 10^6 \text{ Hz}}\end{aligned}\tag{8}$$

Now for calculating the expected seperation between the O-mode and X-mode cutoff freqency above Tromsø, we subtract the cutoff freqency of the O-mode and X-mode.

$$seperation = \omega_O - \omega_X\tag{9}$$

$$\begin{aligned}&= 5.0 \times 10^6 \text{ Hz} - 2.956 \times 10^6 \text{ Hz} \\ &= \underline{2.044 \times 10^6 \text{ Hz}}\end{aligned}\tag{10}$$

So the expected seperation between the O-mode and X-mode is $2.044 \times 10^6 \text{ Hz}$.

2.5 Two circularly polarized electromagnetic waves

An HF radar operating at 5 MHz sends a linearly polarized radio wave into the vertical direction. The radar observes two circularly polarized electromagnetic waves at different time group delays. Explain what is going on.

When a HF radar operating at 5MHz sends a linearly polarized radio wave into the vertical direction and observes two circularly polarized electromagnetic waves at different time group delays.

The ionosphere has two different refractive indices for two different polarizations, the most common ones are the ordinary (O-mode) and the extraordinary mode (X-mode). The single linearly polarized radio wave consists of two circular polarization waves. This comes from the fact that the sum of two circular polarizations is a linear polarization hence we can send a linearly polarized radio wave and receive a circularly polarized radar echo. Expressed as:

$$\frac{1}{2} \begin{bmatrix} 1 \\ i \end{bmatrix} + \frac{1}{2} \begin{bmatrix} 1 \\ -i \end{bmatrix} = \begin{bmatrix} 1 \\ 0 \end{bmatrix} \quad (11)$$

Which will be the O-mode and the X-mode, these modes have different group velocities and refractive indices. This means that the two modes can separate and can arrive at different delays. The reason for O-mode and x-mode is that we have two solutions to the dispersion relationship for EM waves in magnetized plasma. Regarding what is mentioned earlier, the different polarizations will have different propagation paths through the ionosphere as shown below.

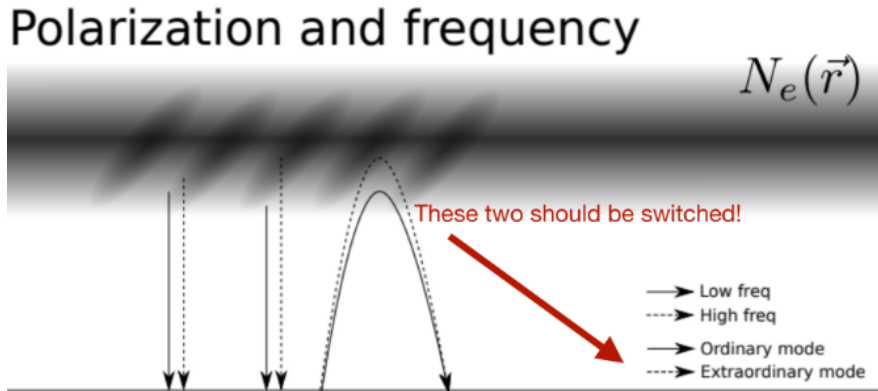


Figure 6: Image from lecture slides: Ionosondes p.36

2.6 Automatically scaled foF2 correct?

Go to the GIRO database and find the Millstone Hill digisonde sounding corresponding to 2024-01-02 00:45:00UT. Is the automatically scaled foF2 correct? If not, what should it be?

At the table to the left of the plot in figure 7, we see that the foF2 is set to 4.700MHz. But when looking at the plot we see, that it is approximately 5.5MHz.

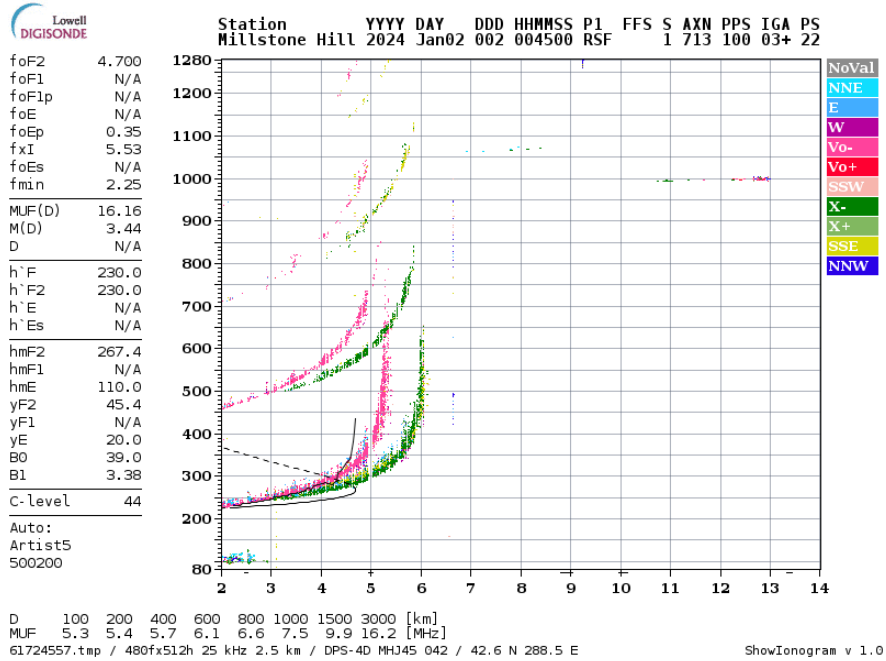


Figure 7: GIRO data plot

2.7 foF2 parameter scaled wrong again

Is the foF2 parameter correctly scaled by the digisonde automatic scaler? If not, what would be a more correct value?

Same again we can see that the plot down below is wrong again. The table is showing that the foF2 is 4.425MHz, but the plot show that it is about 5.5MHz.

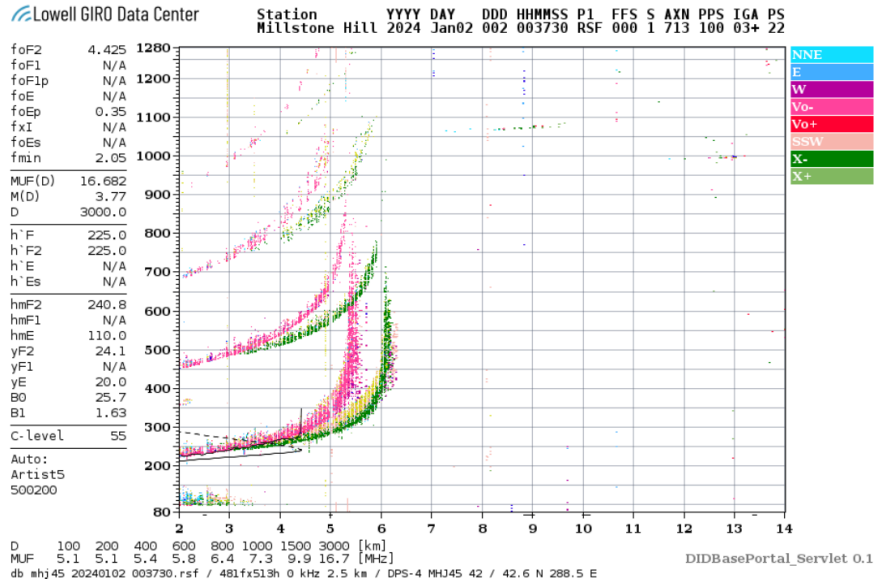


Figure 8: GIRO data plot

2.8 HF sounding of the ionosphere

Explain how HF sounding of the ionosphere can be used to monitor radio propagation conditions for HF telecommunications on transpolar flights.

HF sounding of the ionosphere can be used to monitor radio propagation conditions for HF telecommunications on transpolar flight. This works through ionospheric reflections, this ionospheric reflection comes from when the electromagnetic wave frequency matches the plasma frequency.

Recall that the total reflection at an interface of two media occurs when the phase velocity approaches infinity on the other side of the interface boundary, this happens when $n \rightarrow 0$.

2.9 electron density profile

Use the IRI model to obtain an electron density profile over Tromsø, Norway on 2016-07-07T12:00:00.

2.9.1 foF2 parameter in an ionogram

What would the foF2 parameter in an ionogram be based on the electron density profile.

As we know the **foF2** parameter, tells us the peak electron density of the F2-region of the ionosphere. This means that the foF2 parameter in an ionogram will be based on the maximum electron density, as shown in plot 9.

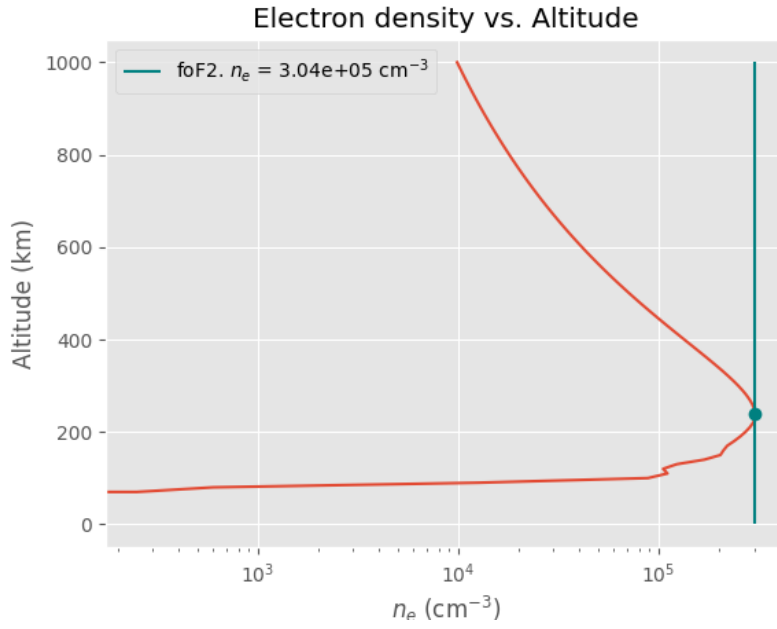


Figure 9: Data from IRI model, plotted with electron density on the x-axis and altitude on the y-axis where the foF2 parameter is marked.

2.9.2 O-mode wave propagating

Calculate the phase velocity of the O-mode wave propagating in the vertical direction as a function of height up to the reflection altitude. Use 200 frequencies evenly spaced between 0.5 and 16 MHz.

Figure 10 shows the phase velocity of the O-mode wave propagation. We can see that as the refraction, gets less we have a higher phase velocity which correlated good with having the phase velocity defined as.

$$v_p = \frac{c}{n} \quad (12)$$

Where n is the refractive index given by the Appleton-Hartree formula, defined as.

$$n = \sqrt{1 - \frac{\omega_p^2}{\omega^2}} \quad (13)$$

where angular electron plasma frequency $\omega_p^2 = \sqrt{e^2 n_e / \epsilon_0 m_e}$ and angular frequency of radio wave $\omega = 2\pi f$.

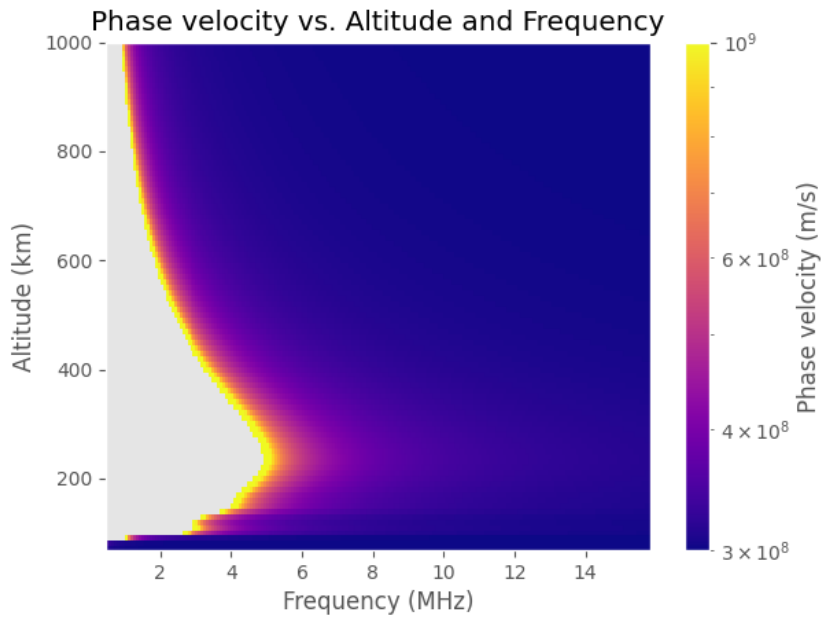


Figure 10: O-mode wave propagating in the vertical direction as a function of height up to the reflection altitude.

```

1 # Frequency range [0.5, 16] MHz
2 frequency = np.linspace(0.5e6, 16e6, 200)*2*np.pi
3 omp2 = (cons.e**2.0 * n_e / (cons.epsilon_0 * cons.electron_mass)) #
4     Angular electron plasma frequency
5
6 phase_vel = []
7 for freq in frequency:
8     vp = cons.c / np.sqrt(1 - (omp2 / freq) ** 2) # phase velocity
9     phase_vel.append(vp)
10
11 for i, freq in enumerate(frequency):
12     plt.pcolormesh((frequency/2*np.pi)/1e7, alt_km, np.array(phase_vel).T,
13                     cmap="plasma", shading="auto", vmin=3*1e8, vmax=1e9, norm ="log")
14 plt.colorbar(label="Phase velocity (m/s)")
15 plt.title("Phase velocity vs. Altitude and Frequency")
16 plt.xlabel("Frequency (MHz)")
17 plt.ylabel("Altitude (km)")
18 #plt.ylim(68, 1000)
19 plt.show()

```

Listing 3: code for calculating the phase velocity of the O-mode wave propagation

2.9.3 O-model reflection altitude

Indicate what is the O-mode reflection altitude.

In the figure below, we have indicated where the O-mode cut-off frequency is. This means that we have an O-mode reflection altitude of about 240km.

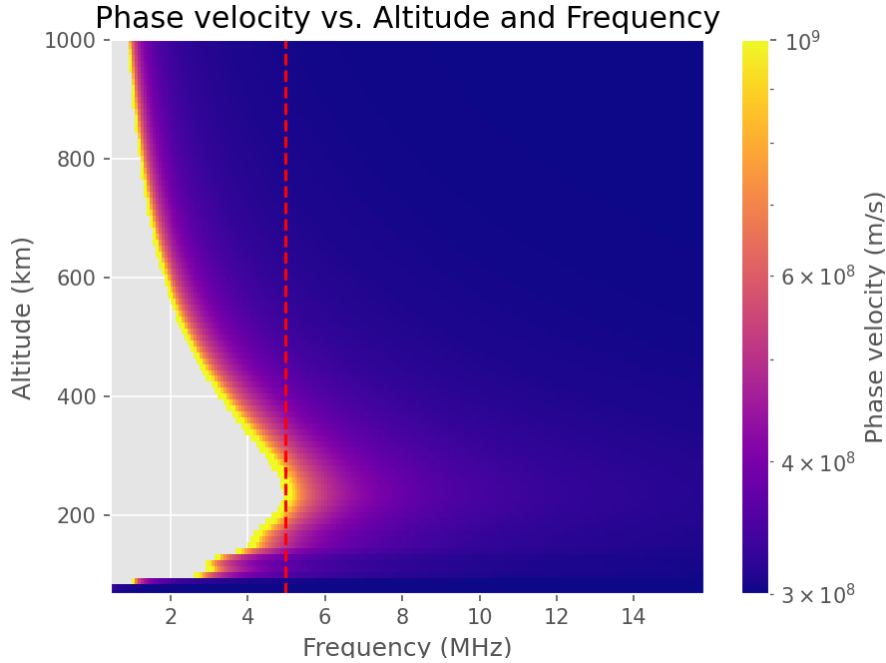


Figure 11: O-mode cut-off frequency

2.9.4 Calculate the group velocity of the O-mode wave

Calculate the group velocity of the O-mode wave as a function of height up to the reflection height (ignore magnetic field and collisions). Use 200 frequencies evenly spaced between 0.5 and 16 MHz

In the figures below we have the group velocity of the O-mode wave as a function of height up to the reflection height, where we have used 200 frequencies evenly spaced between 0.5 and 16MHz. This gives an average group velocity of $2.7 \cdot 10^8 \text{ m/s}$. We see at approximately 5MHz the reflection height goes to infinity, as the frequencies above this propagate through the ionosphere into space, as they are not reflected by the ionosphere.

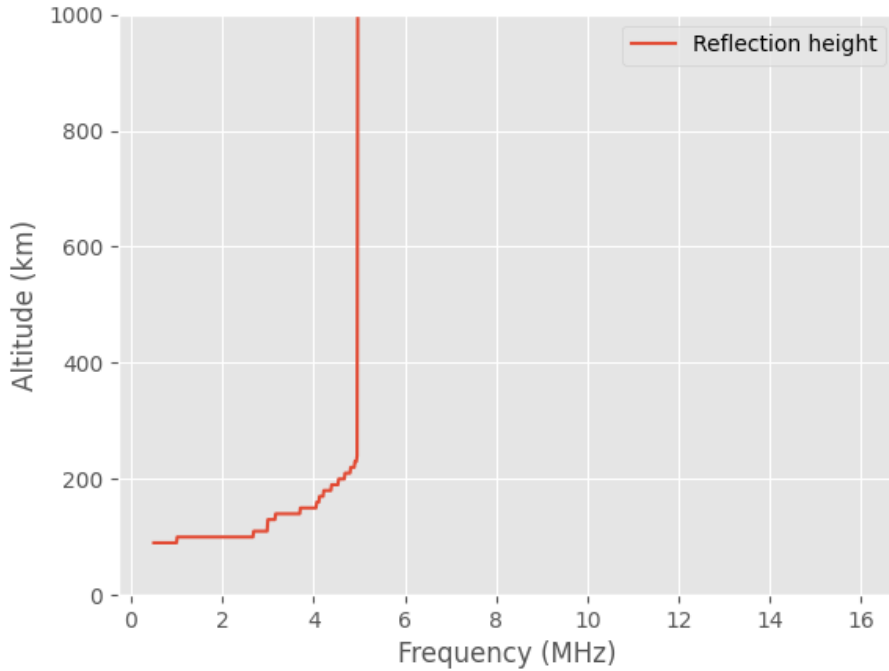


Figure 12: Plot of the group velocity of the O-mode wave as a function of height up to the reflection height.

We know that when the refractive index grows bigger than 0, we have a reflection of the waves and when it's negative we have no reflection. So for calculating the *group velocity*, we use that.

$$v_g^{-1} = \left(\frac{d}{d\omega} \frac{n\omega}{c} \right) = \frac{1}{cn} \quad (14)$$

```

1 freqs=np.linspace(0.5e6, 16e6, 1000) # frequency range
2 V = np.zeros([len(alt_km), 1000]) # array for refractive index
3 for i in range(len(freqs)):
4     V[:,i] = np.sqrt(1 - omega_p**2/((2.0*np.pi*freqs[i])**2.0)) # refractive
      index
5
6 average_V = np.nanmean(V) # avg refractive index
7 group_velocity = cons.c * average_V # group velocity
8 print("Group velocity:", group_velocity)
9
10 reflection_height = np.zeros(len(freqs), dtype=int) # reflection height for
      each frequency
11 group_delay = np.zeros(len(freqs)) # group delay for each frequency
12
13 dx=np.diff(alt_km)[0]*1e3 # altitude step in meters
14
15 # Reflection height and group delay for each frequency in the range [0.5,
      16] MHz

```

```

16 for i in range(len(freqs)):
17     ridx = np.where(np.isnan(V[:,i]))[0] # reflection index
18     if len(ridx)>0: # if there is a reflection
19         reflection_height[i] = ridx[0] # reflection height for each
frequency
20         group_delay[i] = 2.0*np.sum(1/(cons.c*V[0:(ridx[0]-2),i])*dx) #
group delay for each frequency
21     else: # if there is no reflection
22         reflection_height[i] = -1 # reflection height
23         group_delay[i] = -1 # group delay
24
25 plt.plot(freqs/1e6, alt_km[reflection_height], label="Reflection height")
26 plt.xlabel("Frequency (MHz)")
27 plt.ylabel("Altitude (km)")
28 plt.ylim([0,1000])
29 plt.legend()
30 plt.show()

```

Listing 4: code for calculating the group velocity of the O-mode wave as a function of height up to the reflection height

2.10 O-mode trace simulated

Use the results of the previous task to simulate the O-mode trace of the ionogram that would result from the electron density profile. You will need to estimate the group delay from transmit to reflection, and back. The total group delay will be twice the group delay from the transmitter to the reflection altitude. You can use the refractive index that includes no magnetic field or collisions. Make a plot of the ionogram.

In figure below we have simulated the o-mode trace of the ionogram that would result from the electron density profile. For calculating the O-mode trace (virtual height), we need to estimate the group delay from transmission to reflection. Hence, we can define the group delay as.

$$\tau = 2 \int_0^x \frac{1}{cn} dx \quad (15)$$

Here x would represent the reflection altitudes and n is the refractive index (eq.12).

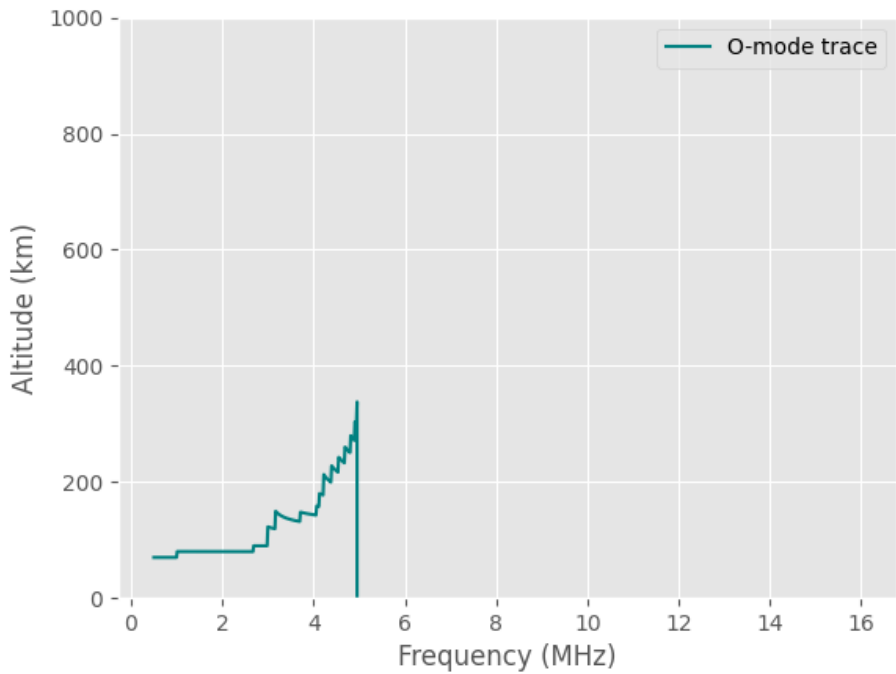


Figure 13: 0-mode trace, or O-mode virtual height

The plot in Figure 14, shows the ionogram and the corresponding reflection height and o-mode trace. We see that the o-mode trace is more than the true height because the group velocity of EM waves in plasma is less than the speed of light in a vacuum.

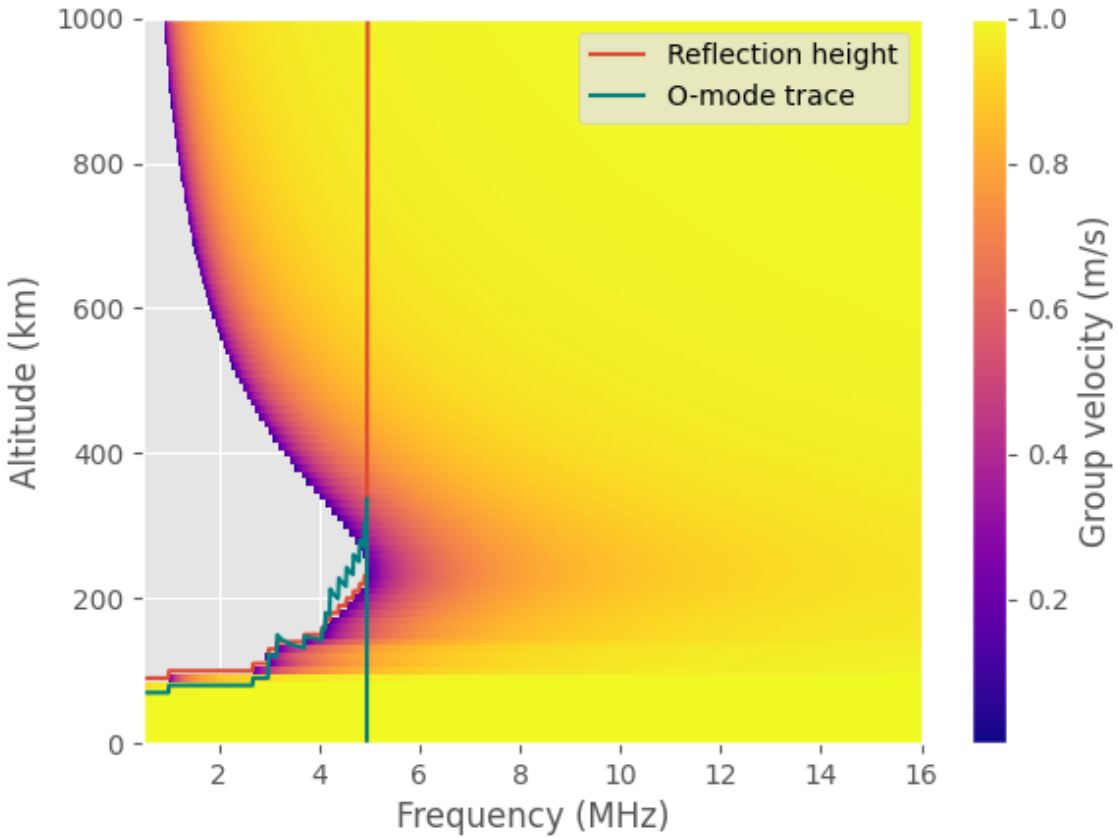


Figure 14: ionogram, with the corresponding reflection height and o-mode trace (virtual height)

```

1 freqs=np.linspace(0.5e6, 16e6, 1000) # frequency range
2 V = np.zeros([len(alt_km), 1000]) # array for refractive index
3 for i in range(len(freqs)):
4     V[:,i] = np.sqrt(1 - omega_p**2/((2.0*np.pi*freqs[i])**2.0)) # refractive
    index
5
6 average_V = np.nanmean(V) # avg refractive index
7 group_velocity = const.c * average_V # group velocity
8 print("Group velocity:", group_velocity)
9
10 reflection_height = np.zeros(len(freqs), dtype=int) # reflection height for
    each frequency
11 group_delay = np.zeros(len(freqs)) # group delay for each frequency
12
13 dx=np.diff(alt_km)[0]*1e3 # altitude step in meters
14
15 # Reflection height and group delay for each frequency in the range [0.5,
    16] MHz
16 for i in range(len(freqs)):
17     ridx = np.where(np.isnan(V[:,i]))[0] # reflection index

```

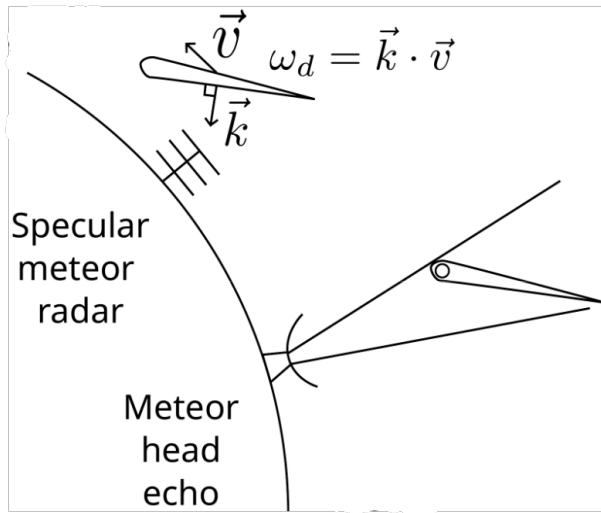
```

18 if len(ridx)>0: # if there is a reflection
19     reflection_height[i] = ridx[0] # reflection height for each
frequency
20     group_delay[i] = 2.0*np.sum(1/(cons.c*V[0:(ridx[0]-2),i])*dx) #
group delay for each frequency
21 else: # if there is no reflection
22     reflection_height[i] = -1 # reflection height
23     group_delay[i] = -1 # group delay
24
25 plt.pcolormesh(freqs/1e6, alt_km, V, cmap="plasma", shading="auto")
26 plt.plot(freqs/1e6, alt_km[reflection_height], label="Reflection height")
27 plt.plot(freqs/1e6, group_delay*cons.c/2.0/1e3, label="O-mode trace",
color="teal")
28 plt.xlabel("Frequency (MHz)")
29 plt.ylabel("Altitude (km)")
30 plt.ylim([0,1000])
31 plt.colorbar(label="Group velocity (m/s)")
32 plt.legend()
33 plt.show()

```

Listing 5: code for calculating the group velocity of the O-mode wave as a function of height up to the reflection height

3 Meteor radar Exercise



3.1 Feature of the measurement containing temperature

An all-sky interferometric meteor radar measures temperatures of the MLT region. What feature of the measurement contains information about temperature?

The key feature of the measurement that contains information about temperature, is the **rate of diffusion** of the meteor trail which is influenced by the atmospheric temperature. As the ionized particles in the meteor trail begin to diffuse into the surrounding atmosphere, the rate at which this diffusion occurs is highly dependent on the temperature of the atmosphere. The radar then measures the rate of diffusion by observing the spectral width of the radar echoes from the meteor's trail. The broader the spectral width, the faster the diffusion, which indicates a higher temperature. On the other hand, a narrow spectral width suggests slower diffusion and thus lower temperature.

3.2 Meteor head echoes and strongest trail echo

Figure 4 contains meteor head echoes from at least seven different meteors. Can you find them? Also identify the strongest specular meteor trail echo in the figure.

In figure 15, we have pointed out seven different meteor head echoes with red arrows. The strongest specular meteor trail echo is going down exponentially from approximately 110km to 90km, which is the head-echo and the part following after is specular. At around 100km we have this gray cloud part, which is non-specular.

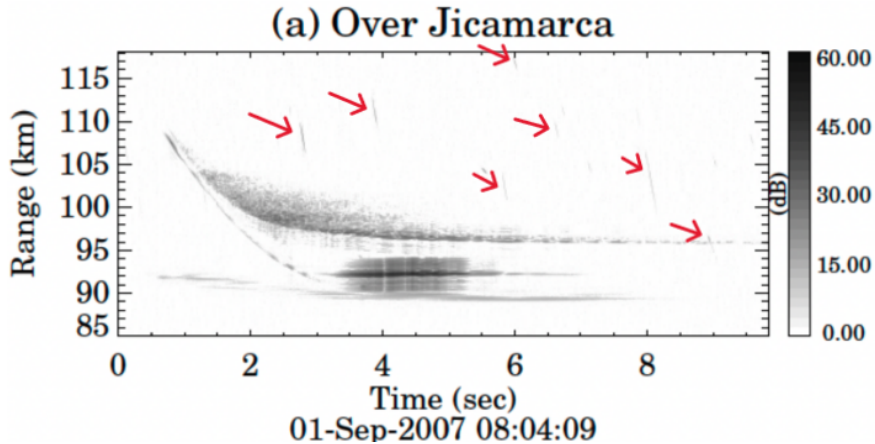


Figure 15: Image from the exercise set

3.3 factors contribute to the mass-loss of meteors

What factors contribute to the mass-loss of meteors during thermal ablation?

The mass loss of meteor during thermal ablation is influenced by several factors related to the interaction between the meteoroid and the Earth's atmosphere. Some factors.

1. *Velocity* of the meteoroid as it enters the atmosphere is crucial. Higher velocities results in greater heating, leading to more rapid ablation.
2. *Size and Density* of the meteorid determine its cross-sectional area and mass per unit volume. Larger and denser meteoroids experience more resistance from the atmosphere, leading to increased heating and mass loss.
3. The *density and composition* of the atmosphere at the altitude of the meteoroids entry affect the ablation.

These are some factors, but we also have factors such as *angle of entry, material composition, ablation efficiency and deceleration and fragmentation*.

3.4 Very slow meteor

A very slow meteor might not be detectable by radar, why is this so?

A radar is in some cases not able to detect a very slow meteor, the reason for this is multiple. First, the radar system relies on the corresponding reflection of radio waves of the ionized meteor tail, when a meteor is moving (very) slowly it will be a possibility that the reflection is not strong enough and get mixed up with background noise. second, the ionization trail behind the meteor reflects radar waves, this is proportional to the speed of the meteor. at last, as the meteor is moving slowly it would be more effected by the neutral wind.

3.5 Hyperbolic orbit

If a meteor is seen traveling at 100 km/s relative to Earth, it is on a hyperbolic orbit (as long as it does not encounter to Sun or planets). Why is this?

If a meteor is seen traveling at 100 km/s relative to Earth, it is on a hyperbolic orbit. As this exceeds the escape velocity of Earth, it can not be an object from Earth. Meaning that it will have an hyperbolic orbit, if the meteor was a object from Earth it would have a **MEO** or **HEO**. In a hyperbolic orbit, the object follows a trajectory that is open and unbounded. Meaning that it will, not return to the region where the body it escaped from is. [4]

3.6 Ionized meteor trail evolution

There are three main different effects that an ionized meteor trail experienced after it has been formed. What are they?

The three main effects that an ionized meteor trail experience after it has been formed, it first "recombination", secondly ambipolar diffusion and lastly turbulent diffusion. In the "recombination" stage of the meteor trail, we will have plasma drift with neutral flow velocity (wind). In the second stage, we have **ambipolar diffusion** which expands the trail, in which both ions and electrons diffuse together under the influence of pressure and temperature gradients. As for the last stage, we have **plasma turbulence development** (turbulent diffusion).

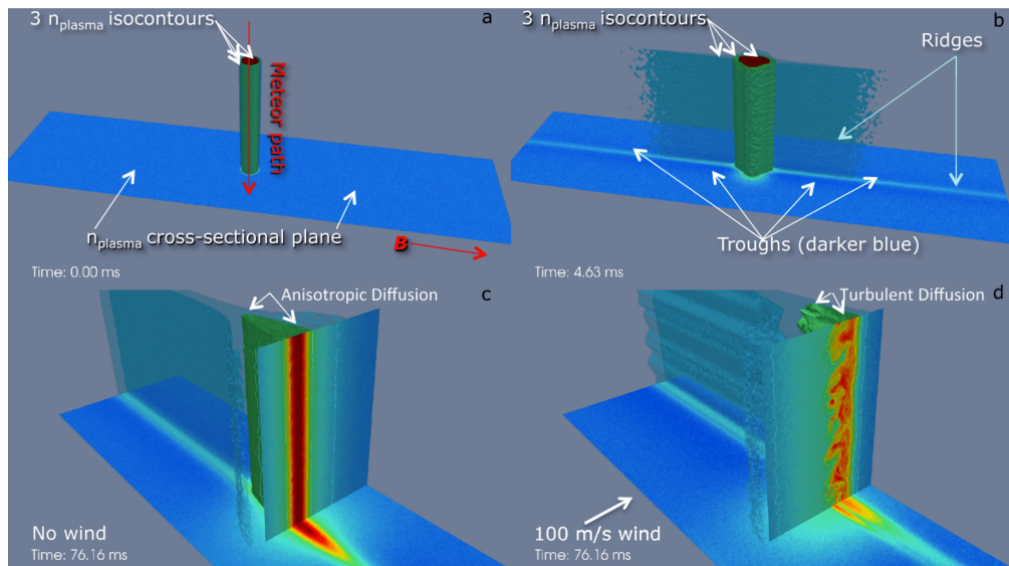


Figure 16: Evolution of a ionized meteor trail, from the lecture slides.

3.7 Sinusoidal oscillations and five different phases

Figure 17 shows a specular meteor trail echo measured with the SIMONe Germany radar system. There are five channels from different receiver antennas that show the complex voltage of the echo. What is causing the sinusoidal oscillations in the received signal? Why do each of the five channels appear to have a different phase?

The reason for the sinusoidal oscillations in the received signal, comes from the interference with the transmitted signal. As the reflected signal interferes directly with the transmitted signal, it leads to constructive and destructive interference pattern which is seen as a sinusoidal oscillations.

As the five different receivers sees the same specular trail echos from the same meteor. The conditions for specularity is met at different times for the different transmit-receive paths, meaning that it will appear as the five channels have different phases.

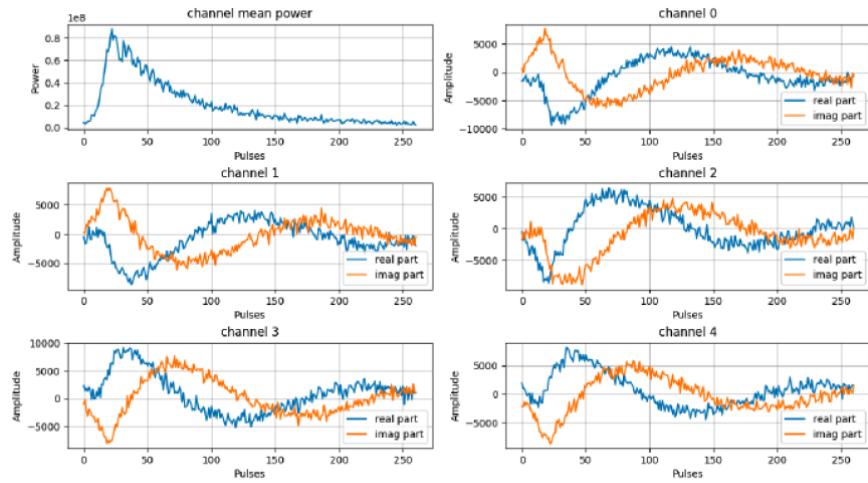


Figure 17: Specular meteor trail echo measured with five interferometer antennas (M. Clahsen, MSc Thesis 2017).

3.8 Estimate the zonal and meridional winds

There is code and a data file under <https://github.com/jvierine/fys3002/tree/main/smr>. The file `read_smr_data.py` shows how to read Doppler shifts of specular meteor trail echoes. The file contains the Bragg wave vectors \vec{k}_b for each trail echo. All trail echo measurements are between 93 and 96 km heights and during a 15 minute time span. Estimate the zonal and meridional winds. You can compare your result with the mean wind estimates show in the file `mean_wind.png`. If you are interested, you can also use the full dataset for one full day of measurements at all altitudes `mmaria_multilink_mmaria-norway_20230101.h5` and derive the mean wind as a function of time and height, as shown in the image `mean_wind.png`.

We can use the Doppler shift of specular meteor trail echoes to study the neutral wind of the MLT region where meteors ablate. For calculating the zonal mean wind and the meridional mean wind, we have the Bragg wave vectors \vec{k}_b components for each trail echo and the same with the Doppler shift measurements (r). We then have a matrix vector representation, defined as.

$$m = Ax \longrightarrow \begin{bmatrix} r_1 \\ r_2 \\ \vdots \\ r_N \end{bmatrix} = \begin{bmatrix} k_1^x & k_1^y \\ k_2^x & k_2^y \\ \vdots & \vdots \\ k_N^x & k_N^y \end{bmatrix} \begin{bmatrix} \bar{u} \\ \bar{v} \end{bmatrix} \quad (16)$$

Here \bar{u} is the zonal mean wind and \bar{v} is the meridional mean wind. We can statistically estimate the mean wind velocity using the method of least-squares.

$$x_{ML} = (A^T \Sigma^{-1} A)^{-1} A^T \Sigma^{-1} m \quad (17)$$

You will find the code snippet for calculating this below. By calculating this we get that zonal mean wind is **-10.423m/s** and the meridional mean wind is **6.485m/s**. This seems a little bit low compared with the plot in Figure 18, where the wind velocity reaches 150m/s. I would expect that our calculated velocities would reach something like 80m/s and vice-versa.

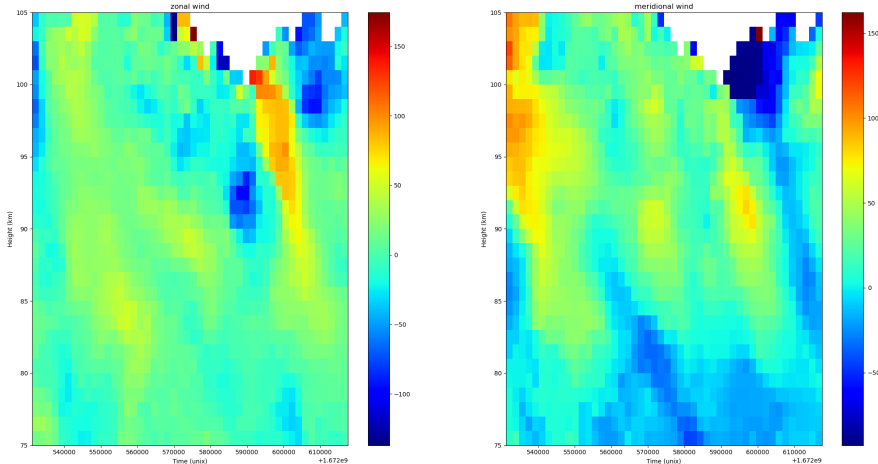


Figure 18: Mean wind plot, with full day of measurements, link to GitHub image

```

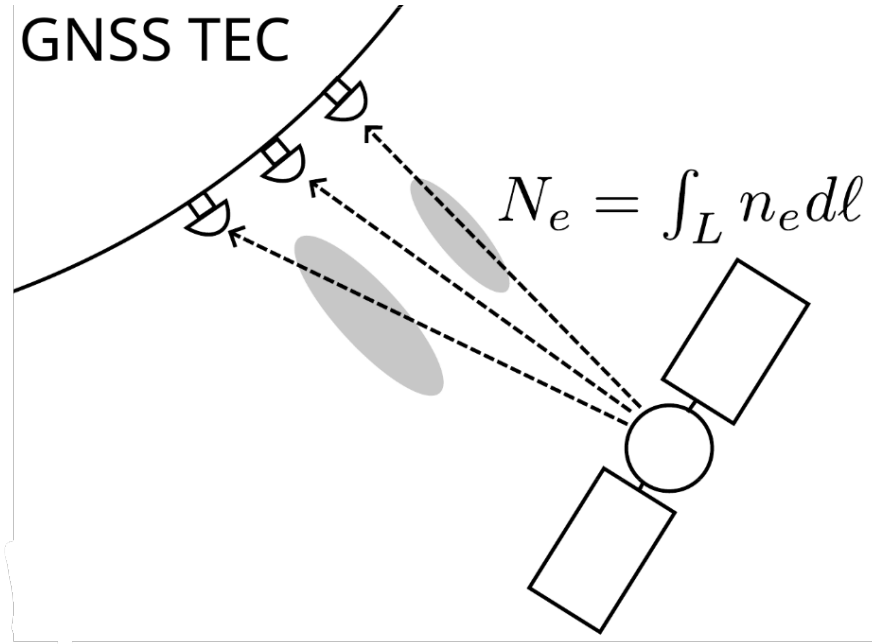
1 def wind_est(doppler, k_north, k_east):
2     A = np.array([k_north, k_east]).T
3     # Calculate covariance matrix of A
4     sigma = np.cov(A)
5     # Calculate the inverse of the covariance matrix
6     sigma_inv = np.linalg.pinv(sigma)
7     # Calculate the pseudo-inverse of the matrix product A^T * sigma_inv * A
8     A_pseudo_inv = np.linalg.pinv(A.T @ sigma_inv @ A)
9     # Estimate the wind vector using the maximum likelihood method
10    x_ml = A_pseudo_inv @ A.T @ sigma_inv @ doppler

```

```
11     return x_ml  
12  
13 wind_vector = wind_est(doppler, k_radar_north, k_radar_east)  
14 print("Estimated wind vector (zonal, meridional):", wind_vector)
```

Listing 6: code for estimate the zonal and meridional winds

4 Total Electron Content (TEC)



4.1 Ionospheric contribution to measured distance (pseudorange)

You are tasked by the Norwegian space Agency (NoSA) to evaluate design for a satellite based positioning systems that only uses one frequency. The three competing designs have frequencies of 50 MHz, 233 MHz and 1.5 GHz. You know that the ionospheric plasma slows down the electromagnetic wave, resulting with extra distance, if the measured group delay between the satellite and a receiver is converted into distance assuming speed of light in free space. Calculate the ionospheric contribution measured distance (pseudo-range) at the three frequencies. Assume an ionospheric line integrated electron density of 40 TEC units ($10^{16} m^{-2}$). Which frequency would in your opinion be best for location accuracy? why?

The group delay of a signal is the delay expected for free space plus the extra delay caused by the speed of light slowing down when the EM wave interacts with the electrons in plasma. The group delay is a primary measurement of a GNSS receiver, which is derived by using the pseudorandom coded transmissions to determine the group delay between the satellite and the ground station, as well as the clock error of the receiver. We express the group delay as:

$$p(f) = c\tau_g(f) = L + \frac{40.308}{f^2} N_e \quad (18)$$

This is referred to as the pseudorange, which is illustrated in figure 19. We are going to calculate the ionospheric contribution to the pseudorange, we use only the last part of equation 18.

$$D_f = \frac{40.308}{f^2} N_e \quad (19)$$

We can than calculate using frequencies of 50 MHz, 233 MHz and 1.5 GHz.

$$D_{50MHz} = \frac{40.308}{(50 \cdot 10^6)^2} 40 \cdot 10^{16} = 6449m$$

$$D_{233MHz} = \frac{40.308}{(233 \cdot 10^6)^2} 40 \cdot 10^{16} = 296.99m$$

$$D_{1.5GHz} = \frac{40.308}{(1.5 \cdot 10^9)^2} 40 \cdot 10^{16} = 7.16m$$

To consider which frequency that would be best for location accuracy, we need to take into account the delay and reflection of the frequencies. We know that lower frequencies experiences larger delays in the ionosphere compered with the higher frequencies, this comes true by looking at the calculated values above. From the values above, we see that 50MHz and 233MHz is experiencing more delay compered with 1.5GHz. So by choosing 1.5GHz will result in less error in the measured pseudorange and hence be best for location accuracy.

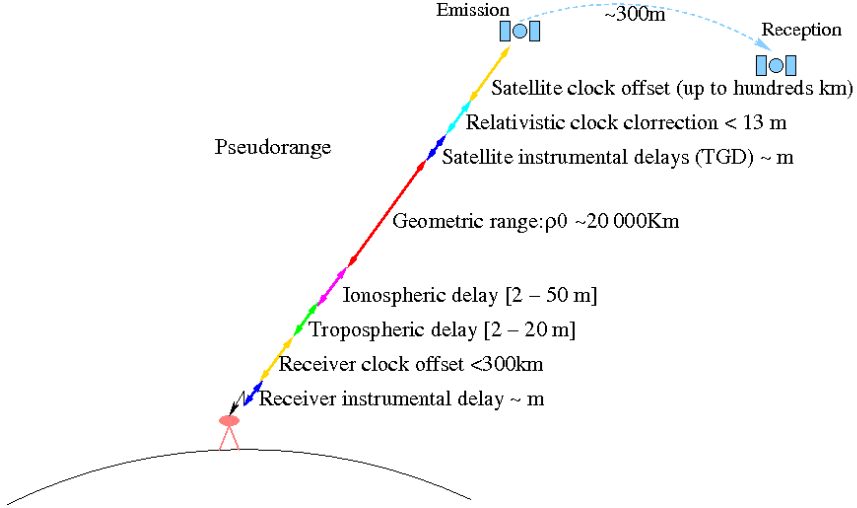


Figure 19: Pseudorange measurements content.[5]

4.2 Errors in ionospheric delay - and TEC measurements

GNSS observations of the ionosphere use an approximate formula for refractive index. How large of a relative error n_1/n in the refractive index is made when using the first-order Taylor series approximation:

$$n_1 = 1 - \frac{\omega_p^2}{2\omega^2} \quad (20)$$

instead of

$$n = \sqrt{1 - \frac{\omega_p^2}{\omega^2}} \quad (21)$$

How large are the errors that result from this approximation in ionospheric delay measurements and total electron content measurements? Evaluate electron densities between $n_e = 10^{10}$ and $n_e = 5 \cdot 10^{12}$ electrons per cubic meter. Evaluate the accuracy of the approximation with two different frequencies: 50 MHz and 1.5 GHz.

For extra credit, you can evaluate how large of a mistake is made by using $n = \sqrt{1 - \omega_p^2/\omega^2}$ instead of the full Appleton-Hartree equation that includes electron collisions and the Earth's magnetic field.

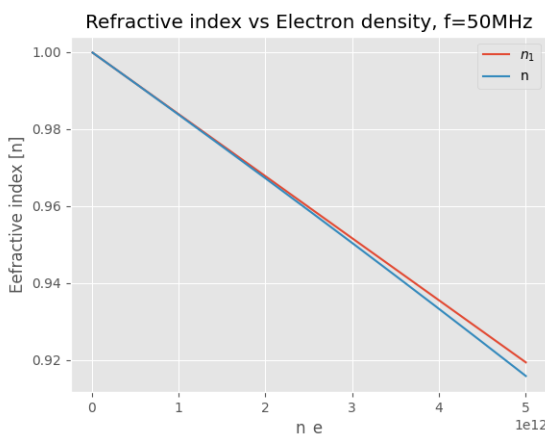
In the equation above we have the *angular frequency of radio wave* ω

$$\omega = 2\pi f$$

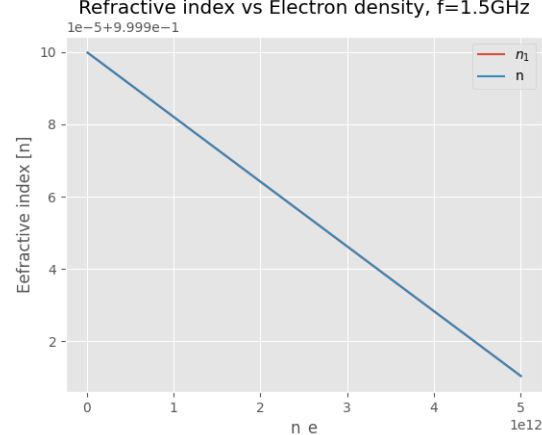
and the *angular electron plasma frequency* ω_p

$$\omega_p = \sqrt{\frac{e^2 n_e}{\epsilon_0 m_e}}$$

Now we can compute the refractive index, using Python as we want to evaluate the electron densities between $n_e = 10^{10}$ and $n_e = 5 \cdot 10^{12}$. Then calculate with frequencies 50 MHz and 1.5 GHz, which gives the following plots.



(a) $f = 50MHz$



(b) $f = 1.5GHz$

Figure 20

We see that when calculating the refractive index with 50 MHz, the error between n_1 and n is bigger than when calculating with 1.5 GHz. When using 50 MHz we have an error of approximately $0.4n$. For $f = 1.5GHz$ it's approximately zero.

Now we going to evaluate how large of a mistake is made by using.

$$n = \sqrt{1 - \frac{\omega_p^2}{\omega^2}} \quad (22)$$

instead of the **full Appleton-Hartree** equation that includes electron collision and Earth's magnetic field, defined as.

$$n^2 = 1 - \frac{X}{1 - iZ - \frac{\frac{1}{2}Y_T^2}{1-X-iZ} \pm \frac{1}{1-X-iZ}(\frac{1}{4}Y_T^4 + Y_L^2(1-X-iZ)^2)^{1/2}} \quad (23)$$

X is the plasma density term, Y_L is the longitudinal electron gyro term, Y_T transverse electron gyro term, and Z is the collision term. By computing the difference between them, we get that we have a difference/mistake of $9.236 \cdot 10^{-12}$. Hence, it's a really small difference between them. But maybe for some cases, this can be important.

```

1 import numpy as np
2 import matplotlib.pyplot as plt
3 import scipy.constants as const
4
5 B = 50000e-9 # Magnetic field strength in Tesla (50 000 nT)
6 theta = 0 # Angle between wave vector and magnetic field in degrees
7 nu_c = 500 # collision frequency for electrons, Hz
8 n_e1 = 1e10 # m^-3
9 n_e2 = 5e12 # m^-3
10 f = 1.5e9 # Hz, frequency of the wave
11
12 omega_c = 1.3e6 # Electron gyrofrequency in Hz (1.3 MHz)
13 def omega_p(n_e): # Plasma frequency
14     return np.sqrt(n_e * const.e ** 2 / (const.m_e * const.epsilon_0))
15 omega = 2*np.pi*f # Hz
16
17 def X(omega, omega_p): # plasma density term
18     return omega_p ** 2 / omega ** 2
19
20 def Y_L(theta): # longitudinal electron gyro term
21     return omega_c/omega * np.cos(theta)
22
23 def Y_T(theta): # transverse electron gyro term
24     return omega_c/omega * np.sin(theta)
25
26 def Z(nu_c, omega): # collision frequency term
27     return nu_c/omega
28
29 n_e = np.linspace(n_e1, n_e2, 1000)
30 def simplified_Appleton(omega, omega_p):
31     return np.sqrt(1 - omega_p**2/omega**2)
32
33 def full_Appleton():
34     Z_value = Z(nu_c, omega) # Calculate Z value first
35     X_value = X(omega, omega_p(n_e)) # Calculate X value
36     Y_T_value = Y_T(theta) # Calculate Y_T value
37     Y_L_value = Y_L(theta) # Calculate Y_L value
38
39     n = np.sqrt(1 - X_value / (1 - 1j * Z_value - ((1 / 2 * Y_T_value **
40         2) / (1 - X_value - 1j * Z_value)) + (1 / 1 - X_value - 1j * Z_value) *
41         (1 / 4 * Y_T_value ** 4 + Y_L_value ** 2 * (1 - X_value - 1j * Z_value
42             ) ** 2)) ** 0.5)

```

```

40     return n
41
42 # calculate the difference between the two methods
43 print("Mean error of refractive: ", np.mean(full_Appleton()/
    simplified_Appleton(omega, omega_p(n_e))))

```

Listing 7: code for estimate simplified and full Appleton-Hartree equation

4.3 Vertical TEC and slant TEC.

Explain the difference between equivalent vertical TEC and slant TEC. Why is vertical TEC useful for ionospheric studies? Additionally, can you explain how the procedure for calculating vertical TEC works?

Equivalent vertical TEC (VTEC) and slant TEC (STEC) are two different ways of representing the total electron content in the ionosphere along a certain path.

VTEC, is independent of the zenith angle so we remove the geometric effect of the slant, Which causes larger TEC. That would say, VTEC represents the total number of electrons in a vertical column above a unit area on the Earth's surface.

STEC, we have kept the geometric effect. This causes the signal to travel a further distance, through the ionosphere and the neutral atmosphere. However, it does not differentiate between the ionospheric and atmospheric contributions along the slant path. So the STEC represents the total number of electrons along the line of sight between a satellite and a receiver.

The vertical TEC is useful for ionospheric studies, as it is vertical hence, as the slant TEC paths travel a longer distance through the ionosphere they are more affected by perturbations and the effect of the neutral particles and plasma that can cause errors. We have a vertical propagation path through the ionosphere.

The procedure for calculating vertical TEC or scaling slant TEC to vertical TEC involves using a mapping function. The mapping function is the assumed shape of the ionospheric electron density profile. Hence, the vertical equivalent TEC estimate is.

$$\hat{N}_e(0) = N_e(\alpha) \frac{s(0)}{s(\alpha)} \quad (24)$$

where $N_e(\alpha)$ comes from the slant TEC, which includes the geometric term $s(\alpha)$ and an altitude shape assumption.

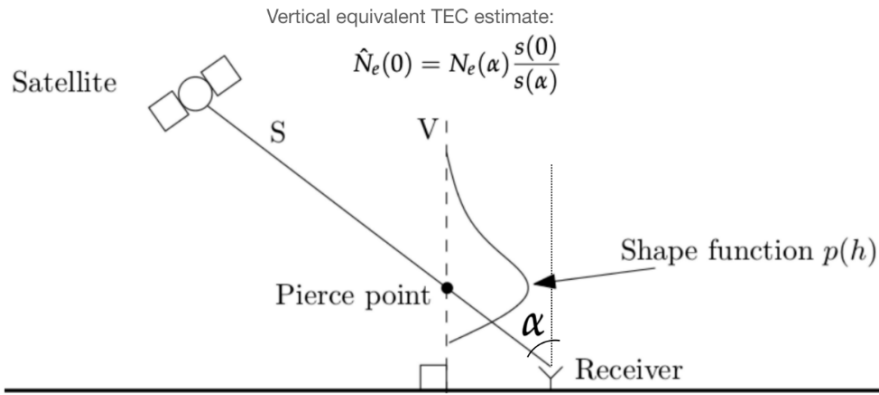


Figure 21: Figure from the lecture notes, "Total electron content slides".

4.4 Errors in vertical TEC from slant TEC

Errors in estimating equivalent vertical TEC from slant TEC tend to be larger for larger zenith angles. Why does this occur?

When estimating equivalent vertical TEC from slant TEC tend, we get larger errors for larger zenith angles. This is due to increased path length through the ionosphere, greater electron density variations, and deviations from vertical propagation assumptions. The first reason, we know that the thickness of the ionospheric layer increases with larger zenith angles, meaning the signal path traverses through a greater distance of the ionosphere. Which can be seen from the slant TEC estimation:

$$N_e(\alpha) = \int_{L(\alpha)} n_e(\vec{\ell}) d\vec{\ell} = n_0 s(\alpha) \quad (25)$$

Secondly, as the path is greater, we will encounter more significant variations in electron density, perturbations, and effects of plasma. At last, the integration path length of the signal through the ionosphere increases with larger zenith angles. This longer path length amplifies the effects of ionospheric irregularities and electron density gradients along the signal path.

4.5 Differential TEC

Space physicists like using differential TEC for studies of ionospheric structure. Can you explain how differential TEC is obtained from vertical TEC?

We can obtain the differential TEC from the vertical TEC, we just high-pass filter what we obtained from the vertical TEC and that is what we call the differential TEC (dTEC). This method is widely used in studies of ionospheric perturbations, such as TIDs, solar flares, blast waves, and polar cap patches.

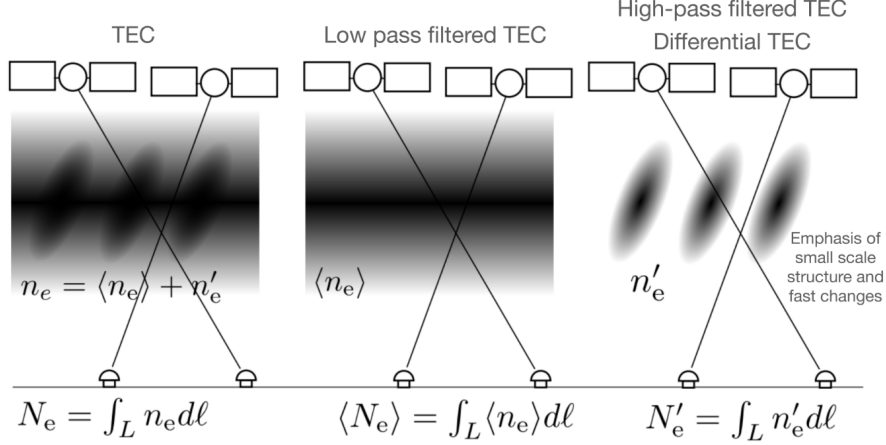


Figure 22: Figure from lecture notes, "Total electron content slides".

4.6 Line integral of electron density

A radio wave that travels through the interstellar medium slows down due to the interaction between the electric field of the electromagnetic wave and free electrons within the medium. A radio astronomer observes a fast radio burst at time t_0 at frequency $f_0 = 1500MHz$ and at time t_1 with the frequency of $f_1 = 1300MHz$. The time difference is measured to be $t_1 - t_0 = 0.2s$. What is the line integral of electron density between the emitting astrophysical object and the Earth? Use units of electrons per square meter. How many TEC units is this? Can you figure out what this is in units of parsec per cubic centimeter? Does Earth's ionosphere significantly contribute to the group delay of the fast radio burst signal observed using a ground-based radio telescope?

We start by calculating the line integral of electron density between the emitting astrophysical object and the earth. Which is given as follows, as a Taylor series expands.

$$\tau_g(f) = \frac{1}{c} \left(L + \frac{40.308}{f^2} N_e \right) \quad (26)$$

Then using the difference that is measured, and solving for N_e .

$$\tau_1 - \tau_0 = \frac{1}{c} \left(L + \frac{40.308}{f_1^2} N_e \right) - \frac{1}{c} \left(L + \frac{40.308}{f_0^2} N_e \right) \quad (27)$$

$$\tau_1 - \tau_0 = \frac{1}{c} \left(\frac{40.308}{f_1^2} N_e - \frac{40.308}{f_0^2} N_e \right) \quad (28)$$

$$\tau_1 - \tau_0 = \frac{1}{c} 40.308 N_e \left(\frac{1}{f_1^2} - \frac{1}{f_0^2} \right) \quad (29)$$

$$N_e = \frac{0.2c}{40.308(f_1^{-2} - f_0^{-2})} \quad (30)$$

$$N_e = 1.01 \cdot 10^{25} \text{ electrons/m}^2 \quad (31)$$

This is equal to the following value in TEC units

$$N_e = 10^{25} - 10^{16} \approx 10^9 \text{ TECU} \quad (32)$$

Which will be the following in nits of parsec per cubic centimeter.

$$N_e = \frac{10^9}{3 \cdot 10^6} \approx 333 \text{ parsec/cm}^{-3} \quad (33)$$

Our ionosphere's total electron content varies a lot, normally a variation around 40 TECU. Besides this, measured TEC units span from around zero to approximately 100 (e.g. geomagnetic storms). This means TEC will absolutely have something to say on our signal from the transmitter to the receiver. Regarding Earth's ionosphere contribution to the group delay of the fast radio burst signal observed using a ground-based radio telescope, we speak of a measured value of 1200DM ($\approx 4 \cdot 10^9 \text{ TECU}$). The TEC unit around 40, will not contribute a lot.

4.7 Pseudorange and carrier phase for observing ionospheric TEC

What is carrier phase and pseudorange measured by a GNSS receiver? What are the pros and cons of using pseudorange and carrier phase for observing ionospheric total electron content?

Carrier phase is a more precise measurement of the phase of the carrier wave transmitted by the satellite. It measures the range between a satellite and a receiver expressed in units of cycles of the carrier frequency, this type of measurement can be made with very high precision (order of millimeters). The Carrier phase is defined as.

$$\Phi(f) = L - \frac{40.308}{f^2} N_e \quad (34)$$

Pseudorange measures the time it takes for a signal to travel from a satellite to the receiver. It's called "pseudo" as it includes errors such as clock, in the receiver and satellite, atmospheric delays, and other sources of ranging error.

$$p(f) = c\tau(f) = L + \frac{40.308}{f^2} N_e \quad (35)$$

Pros of using pseudorange, is that it is pretty straightforward to obtain and is available from most GNSS receivers. Pros of using carrier phase, are that it is way more precise and accurate than pseudorange measurements, making carrier phase measurements more suited for TEC estimation. They are also less affected by the ionospheric delays.

Cons of using pseudorange, is that the measurements are affected by the ionospheric delays which give errors in the measurements. Another con, it has less accuracy compared with carrier phase measurements. The cons of using carrier phase measurements, are it needs of tracking the phase of the carrier signal over multiple cycles.

4.8 Plotting the vertical TEC (St Patrick's Day Storm)

There is a geomagnetic storm on 2015-03-17 (St Patrick's Day Storm). Obtain TEC data from the Madrigal TEC database and visualize it by plotting the vertical TEC onto a map that shows the northern hemisphere polar region. Create a sequence of images that shows the evolution of the geomagnetic storm. You can use either the high resolution line of sight data, or the binned vertical TEC. Can you identify polar cap patches, the tongue of ionization, or expansion of the polar cap in the TEC maps?

In figure 23, we have the TEC data obtained from the Madrigal TEC database. We have visualized the St Patrick's Day Storm (2015-03-17), by having the equator at the center and by showing the northern and southern polar caps. To access the animation, simply click on the images provided and you will be directed to GitHub.

We see at about 07:00 to 08:00 UTC, the tongue of ionization, which extends poleward from the day side storm-enhanced side crossing the polar cap and streaming with the plasma convection flow into the night side ionosphere. This can also be an expansion of the polar cap. Also at around 14:00UTC we also have some polar cap patches, which are "islands" of dense plasma typical with horizontal extensions. we see at about 12 and 16, we have the strongest part of the storm in Europa.

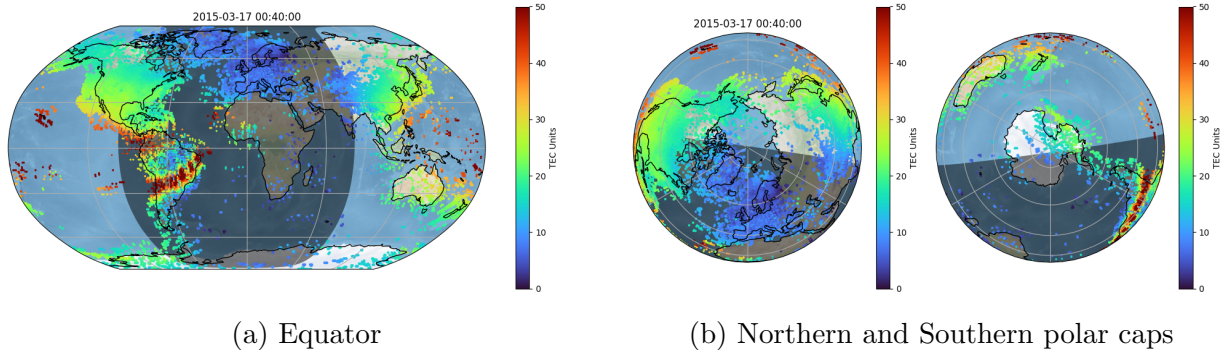
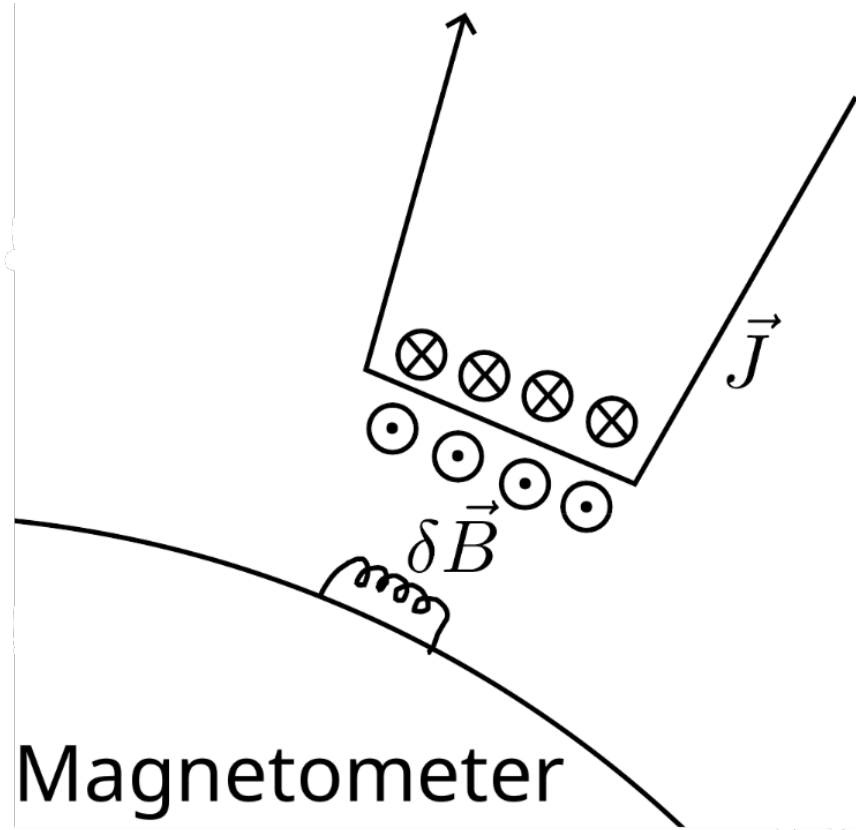


Figure 23: Geomagnetic storm on 2015-03-17. Click on the images for animation or click [here](#).

5 Magnetometer exercises



5.1 Generation mechanisms and typical magnetic flux densities

The Earth's magnetic field can be divided into three components:

$$\vec{B} = \vec{B}_i + \vec{B}_c + \vec{B}_d$$

where the components are the internal, crustal, and disturbance fields. What are the generation mechanisms for these components and what are their typical magnetic flux densities in Tromsø.

The generation mechanism for **internal** magnetic field (\vec{B}_i), is generated primarily by the movement of molten iron within the Earth's outer core. This movement, driven by the convection currents caused by the heat from the inner core, generates electric currents which in turn produce the magnetic field through the dynamo process. It's typical magnetic flux densities in Tromsø is in the range from 50.000nT to 60.000nT.

Generation mechanism for **crustal** magnetic field (\vec{B}_c), is due to rock with different magnetic properties. When the metals are heated they orient according to the internal field. Then when they cool they keep their magnetization for millions of years. It's typical magnetic flux densities in Tromsø is ranging from hundred to a couple of thousand nT.

Generation mechanism for **disturbance** magnetic field (\vec{B}_d), is the part of our measured field that varies on short time scales, from sub-second to days. These variations are caused by external forces such as solar activity, ionospheric currents and etc. Typical in Tromsø this can vary from few to a hundred nT but can increase significantly during geomagnetic storms.

5.2 Fluxgate- and proton precision magnetometers

Two different types of magnetometers are used to make measurement's of the Earth's magnetic field: fluxgate magnetometers, and proton precision magnetometers. Explain the differences between these two instruments. Why are both needed to make accurate measurements of the magnetic field?

Fluxgate magnetometers is a magnetic field sensor for vector magnetic field. It operates by detecting changes in the magnetic flux passing through a core material when it is subjected to an external magnetic field. These changes in flux are then measured and used to determine the strength and direction of the magnetic field.

Proton precession magnetometers (PPM), is the most commonly used magnetometer. Unlike the fluxgate magnetometer, the proton precession magnetometer only measures the total size of the Earth's magnetic field. PPM uses the behavior of protons in a magnetic field. When placed in a magnetic field, proton precess* around the field lines at a frequency proportional to the strength of the field. By measuring the precession frequency, the strength of the magnetic field can be determined.

We are in need of both magnetometers to make accurate measurements of the magnetic field. The reason for this, comes from their capabilities. The fluxgate magnetometers are superior in measuring small changes in the magnetic field over time with precision, hence suitable for long-term monitoring. The proton precession magnetometers provide accurate absolute measurements if the magnetic field strength, easier in use, more handy and cheaper.

5.3 Magnetometer coordinates H, D, Z and I

The magnetic field measured with a ground based magnetometer is often reported with H, D, Z, and I. These coordinates are described e.g., by Laundal and Richmond¹¹. Can you describe what H, D, Z, 11 Karl Magnus Laundal and Arthur D Richmond. Magnetic coordinate systems. Space Science Reviews, 206(1-4): 27–59, 2017 and I are? What values does the magnetic field in Tromsø have for these coordinates? You can use e.g., the IGRF model, or the Tromsø Geophysical Observatory magnetometer data to determine this. How many degrees does the magnetic field direction in Tromsø deviate from vertical?

H is the horizontal component, which represents the strength of the magnetic field in the horizontal plane. It is the component of the magnetic field that is parallel to the Earth's surface. **D** is the declination component, that's represents the angle between the geomagnetic north direction and true north direction at a specific location. **I** is the inclination component, and represents the angle between the magnetic north and the geomagnetic field. It indicates

the angle at which the magnetic field lines intersect the Earth's surface. **Z** the vertical component, and represents the strength of the magnetic field in the vertical direction. It is measured parallel to the geomagnetic field direction.

The magnetic field in Tromsø have the following values for the coordinates.

$$H \approx 10797nT \quad D \approx 8.3266^\circ \quad Z \approx 52789nT \quad I \approx 78.4407^\circ$$

To calculate the deviation of the magnetic field direction from vertical in Tromsø, we will use the inclination (**I**). So to compute this we, can subtract **I** from 90° which gives 11.5593° . Hence the magnetic field direction in Tromsø deviate 11.5593 degrees from the vertical.

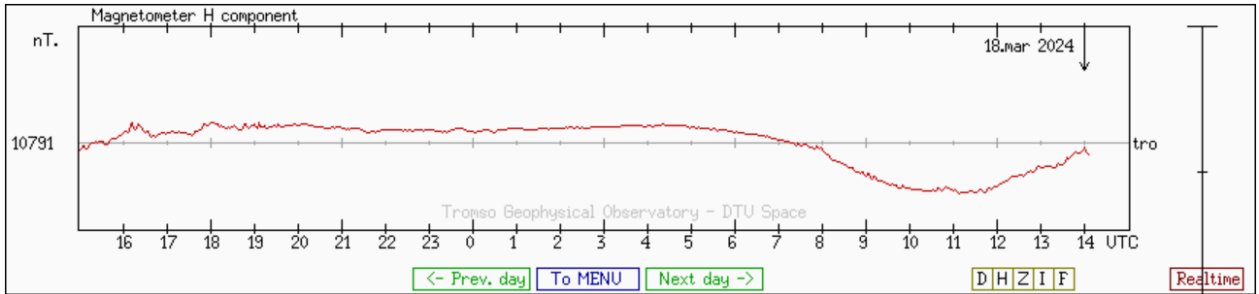


Figure 24: Here is a plot of the horizontal component (H), I didn't manage to add the other components in the same plot.

5.4 challenges when measuring Earth's magnetic field

Explain at least two practical challenges that one might encounter when measuring the Earth's magnetic field.

Two practical challenges that one might encounter when doing measurements of the Earth's magnetic field.

1. External interference

When doing measurements of Earth's magnetic field, we will always have the presence of external interference from various sources. Natural sources such as solar activity, geomagnetic storms, and ionospheric currents can cause temporary variations/disturbances in the magnetic field. Additionally, we can have human-made sources such as power lines, electronic devices, etc.

2. Environmental variability

Earth's magnetic field is subject to spatial and temporal variations as geographic location, altitude, and local geological conditions. As this can vary highly from one location to another, it is challenging to obtain accurate and good measurements in some regions.

5.5 line current and is it westward or eastward?

The Biot-Savart law

$$\vec{B}_d = \frac{\mu_0}{4\pi} \iiint_V \frac{(\vec{J} dV) \times \vec{r}}{|\vec{r}|^3}$$

is used to estimate equivalent currents in the ionosphere that create a magnetic field disturbance. The equivalent current is not necessarily the true current, because this formalism ignores ground-induced currents, and assumptions have to be made about the height and conductivity of the E-region of the ionosphere. For a sufficiently long wire aligned with the x-axis, we can approximately obtain the line current solution:

$$\vec{B}_d = \frac{\mu_0 I}{2\pi |\vec{r}|^2} \hat{x} \times \vec{r}$$

where \hat{x} is the unit vector aligned with the line current, I is the current, μ_0 is the permeability of free space, and \vec{r} is the vector from the line current to the observer. You measure a disturbance magnetic field of $\vec{B}_d = -200\hat{y}$ nT in Tromsø, with \hat{y} being the unit vector towards the local magnetic north. What is the equivalent line current? Assume that a magnetometer is located directly beneath the line current, with the current flowing at an altitude of 110 km. Is the current westward or eastward?

We are given that μ_0 is the permeability of free space ($4\pi \times 10^{-7} T \cdot m/A$), the measured disturbance magnetic field is $\vec{B}_d = -200\hat{y}$ nT and we have an altitude of 110km. In the task, we are given the equation for the disturbance magnetic field, which we can reformulate in terms of the line current solution.

$$\vec{B}_d = \frac{\mu_0 I}{2\pi |\vec{r}|^2} \hat{x} \times \vec{r} \quad (36)$$

This we can express as this.

$$\vec{B}_d = \frac{\mu_0 I}{2\pi r^2} \quad (37)$$

Then express it for the line current I .

$$I = \frac{\vec{B}_d 2\pi r}{\mu_0} \quad (38)$$

$$= \frac{(200 \cdot 10^{-9}) \cdot 2\pi \cdot (110 \cdot 10^3)}{4\pi \cdot 10^{-7}} \quad (39)$$

$$= \underline{\underline{1.1 \times 10^5 A}} \quad (40)$$

As the disturbance magnetic field (\vec{B}_d) is in the negative \hat{y} direction, the current must be in the opposite direction, hence towards the positive \hat{y} direction, which means that the current is eastward. This can be shown through the right-hand rule or by looking at different magnetometer plots for different components.

5.6 Negative or positive disturbance, for Tromsø and Svalbard Magnetometers

The following figure shows estimated equivalent horizontal currents in the ionosphere that are estimated from a network of magnetometers in fennoscandia with magnetometers in the IMAGE magnetometer network. Would the H component of the magnetometer in Tromsø have a negative or positive disturbance at 2023-01-01T00:10:00 UT. What about the magnetometers in Svalbard? Explain your reasoning using horizontal perturbations caused by eastward or westward currents following in the ionosphere. You can check your result using the Norwegian line of magnetometer measurements provided by Tromsø Geophysical Observatory: <https://flux.phys.uib.no/stackplot/>. You can create equivalent current maps using the IMAGE network here: https://space.fmi.fi/image/www/?page=equiv_currents_1D

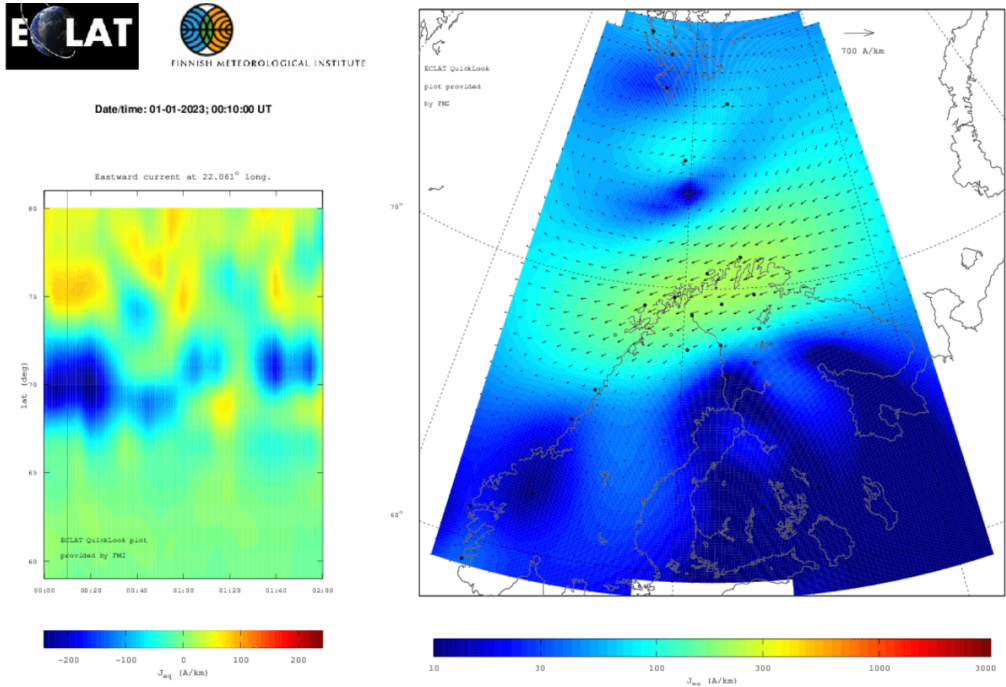


Figure 25: 2D Equivalent Currents

The disturbance in the magnetic field due to ionospheric currents can be understood by using the right-hand rule. If the current flows eastward, the induced magnetic field will decrease the horizontal component of the Earth's magnetic field (negative disturbance), and a westward current will increase the horizontal component (positive disturbance).

When the ionospheric current flows eastward (from west to east), the induced magnetic field from the current will interact with Earth's magnetic field. According to the right-hand rule, the magnetic field induced by an eastward-flowing current will produce a magnetic field component directed downward on the north side of the current and upward on the south side. At the location like Tromsø and Svalbard, which are north of the current's path it will result in a decrease in the horizontal component of the magnetic field because the induced

field opposes the Earth's natural magnetic field.

From Figure 14, we see that we have the vectors pointing down-westwards, this means as stated previously that we will have a negative H component as the vectors oppose the Earth's magnetic field. This also correlated well by looking at the plot in Figure 25. For Svalbard, we have the vectors pointing up-eastwards which will mean that the H-component will be positive. This also correlates well with the plot in Figure 26.

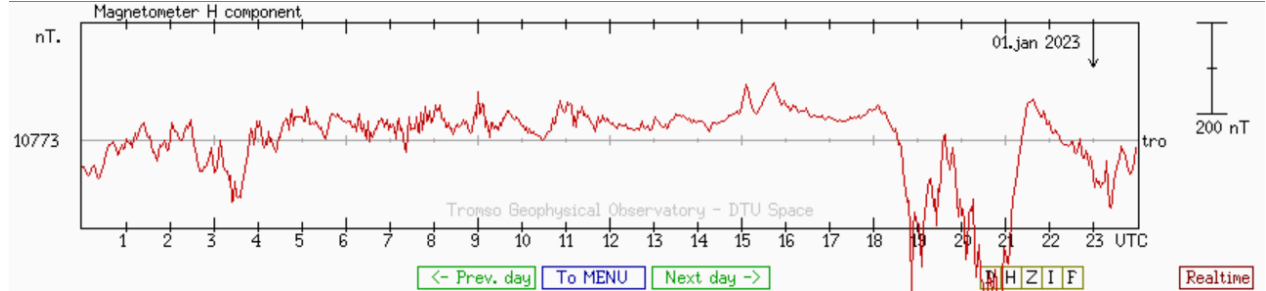


Figure 26: H component of the magnetometer in Tromsø 2023-01-01

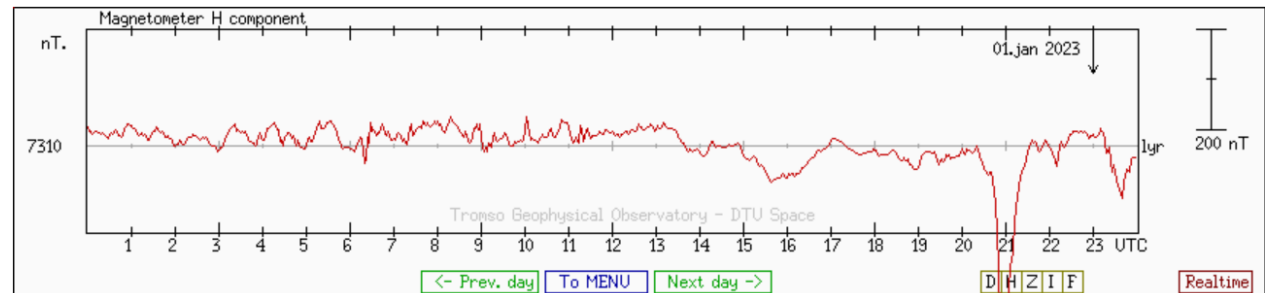
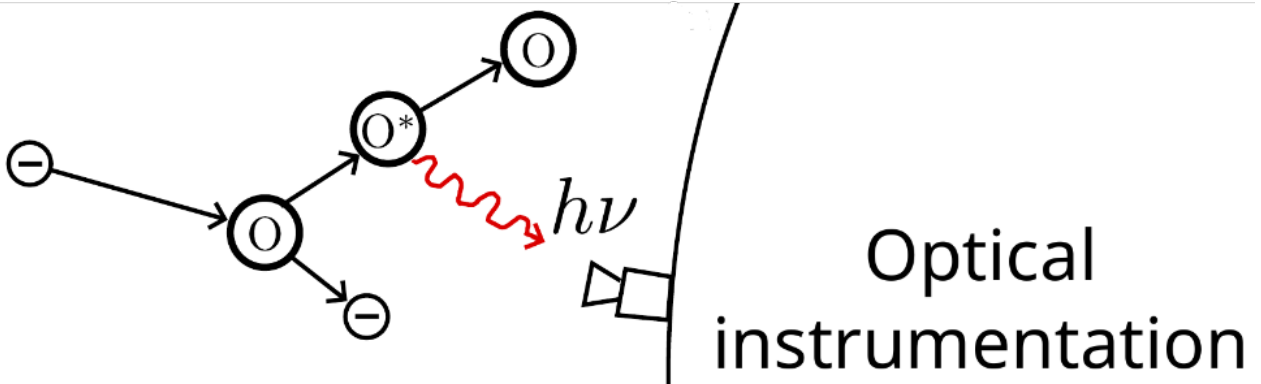


Figure 27: H component of the magnetometer in Longyearbyen 2023-01-01

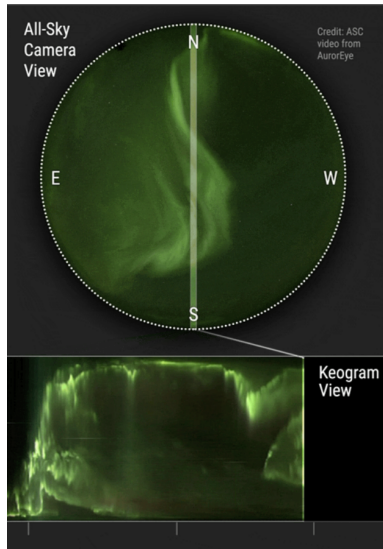
6 Optical Observations



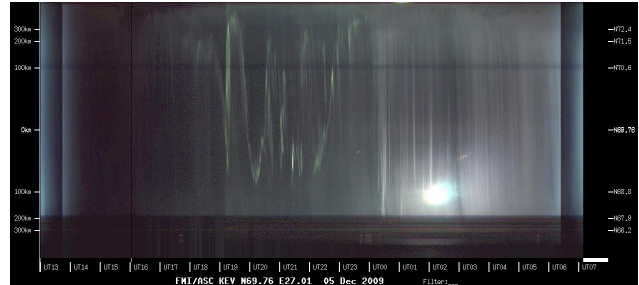
6.1 Keogram

A keogram is used in auroral imaging to provide an overview of auroral activity seen throughout a night of observations. What is a keogram and how is it composed?

Keogram is technique used in auroral imaging, for displaying the auroral activity/intensity throughout a observation. The keogram is composed of a narrow part of a all-sky camera (usually), see figure 28 for illustration. Each of these vertical strips, are arranged chronologically with time progressing form left to right. So the keogram is a time-versus-latitude plot, created from individual images captured during night.



(a) Composition of a keogram



(b) Keogram plot, with labels

Figure 28: Keograms, from Wiki [7] and space.fmi [6]

6.2 Narrow band filters

Why do space physicists use narrow band filters in cameras to study aurora and airglow?

Space physicist uses narrow band filters in cameras, when study aurora and airglow. As the auroras and airglows emit light with various wavelengths across the electromagnetic spectrum, we can use narrow band filters to *isolate specific wavelengths* corresponding to the different emission lines. Like the green parts of the aurora which is atomic oxygen. We also get a better signal to noise ratio, As we usually is all-sky cameras, we receive a lot of noise/pollution from the environment (E.g. the moon) which is broadband. So little of their energy passes through the same narrow band filters. The filters, is looking like this.

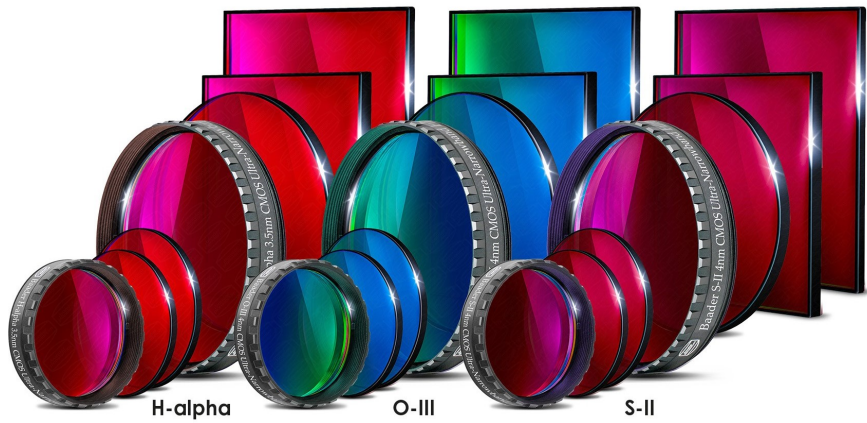


Figure 29: Image from Baader Planetarium

6.3 Magnetic field look direction

The along geomagnetic magnetic field look direction is important for studies of aurora. Why is this the case?

The reasons for, observing/studies of aurora with a look direction that is along the geomagnetic magnetic field. Is important, comes from the electron precipitation and auroral emissions. As the highly energetic electron beams usually is traveling along the magnetic field line direction (*magnetic Lorentz force*). As we get collisions between energetic electrons and neutral atmospheric particles, an optical emission is created which travels along the magnetic field lines.

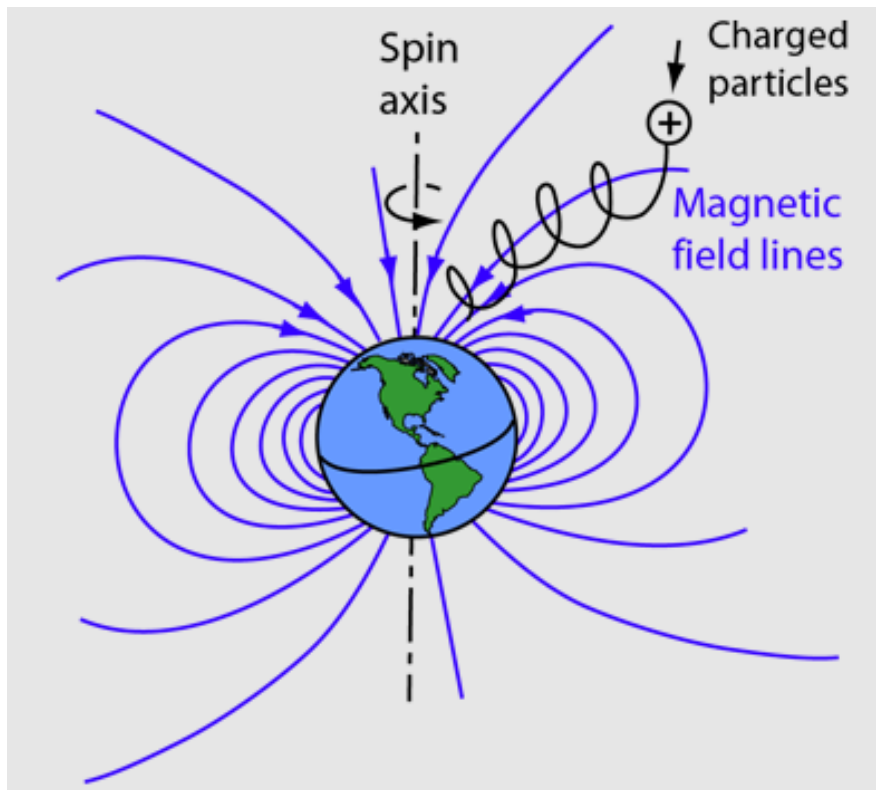


Figure 30: Charged particle traveling along the magnetic field lines.

6.3.1 Three wavelengths for auroral research

Provide at least three wavelengths that are important for auroral research. What excitation states of atoms, molecules or ions do these correspond to?

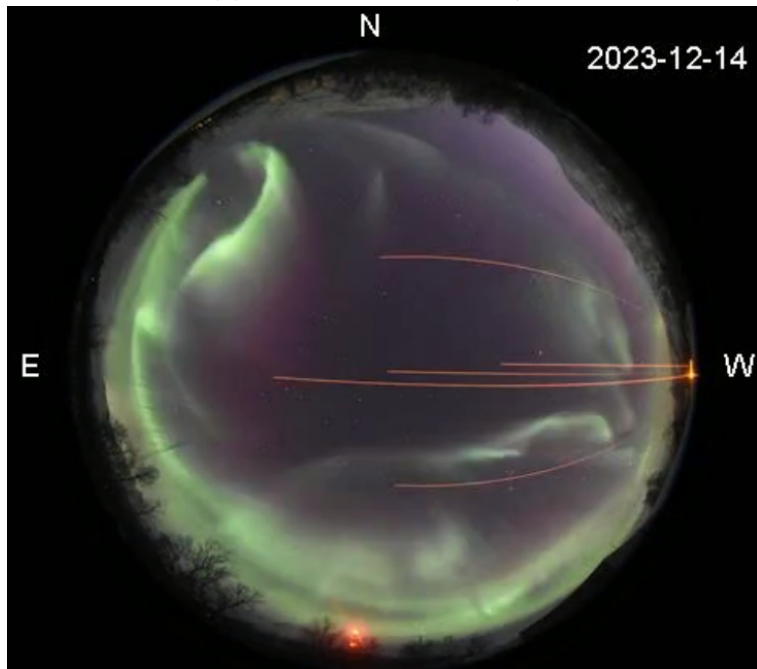
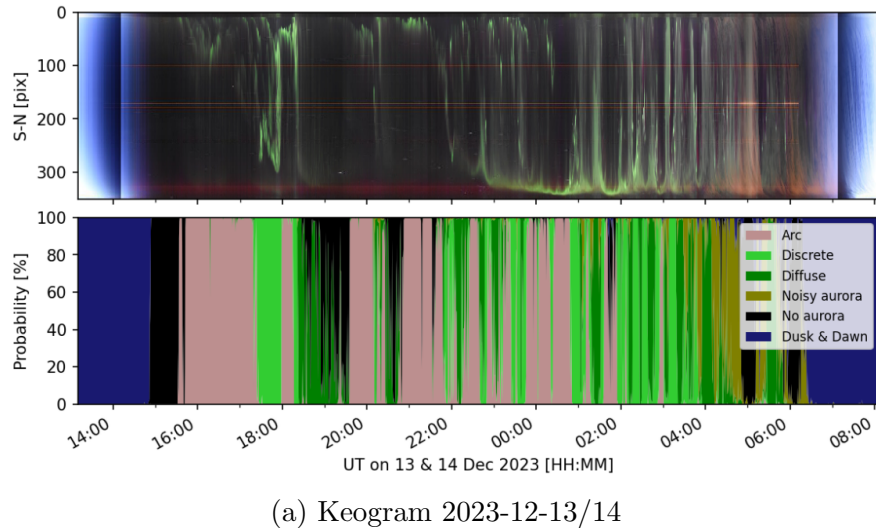
Three wavelengths that are significantly important for auroral research, are 557.7nm (Oxygen green), 630.0nm (atomic oxygen red) and 427.8nm (nitrogen blue/purple). The wavelength 557.7nm emission is created by excited atomic oxygen (O), with the specific transition $^1S_0 - ^1D_2$. For the 630.0nm emission, we have an excitation of atomic oxygen (O) and the corresponding transition $^1D_2 - ^3P_2$. The last 427.8nm emission is created by excited molecular nitrogen ions (N_2^+), which have the transition $B^2 \Sigma_u^+ - X^2 \Sigma_g^+$ (*i think*).

6.4 Interesting auroral event (Tromsø AI)

Go to the Tromsø AI, which is maintained by UEC Japan. Find an interesting auroral event in the database for the 2023 season in Tromsø. Explain what you see. You can ask Björn to explain the auroral event for you. <https://tromsoe-ai.cei.uec.ac.jp//Archive>

In figure 31 you see the auroral event that interested me, which is taken at 13 and 14 December 2023, if you click the all-sky camera image you will be redirected to the movie of

that night. We have a lot of stuff going on this night, but we have distinct three phases of this event the *growth*, *expansion*, and *recovery* phase. We see from the keogram and all-sky camera, that we have a lot of arc auroras forming, while we get a discrete green arc that rises inside it. Then we get some clear diffuse aurora which gets brighter. These type of events is an indication/description of the growth phase which usually starts 1-2 hours before the expansion, for our case it looks like the growth phase has started 5-6 hours before the expansion phase. During the expansion phase, we have drapery, arc, diffuse, rays, and corona structures in our aurora. We can also see the red, pink, and purple bands corresponding to excitations of H, N₂, and O maybe more. For the final (recovery phase) state, which appears to be at around 04:00. We get more noisy aurora.



(b) Image taken from the all-sky camera 2023-12-13/14

Figure 31: Auroral event on 2023-12-13/14. Click on the image for animation

6.5 Calibrate the mapping

How can one calibrate the mapping between a 2d array of image pixel coordinates and the azimuth and elevation angle of an auroral imager?

To calibrate the mapping between a 2d array of image pixel coordinates and the azimuth and elevation angle.

We start by capturing an image of known celestial objects as stars, as they have accurately known celestial coordinates and they will operate as calibration references. We then identify and locate the reference objects in the captured image shown in figure 32. Then we store the pixel coordinates (x, y) of the identified reference points within the image frame. These coordinates represent the location of the reference object in the image plane. As we now have some reference objects, we apply the best-fit mapping functions that relate the image pixel coordinates to the azimuth and elevation angles shown in figure 32. Here it's preferable to have their calculated az-el within $\pm 1/4$ pixels. These mapping functions should account for the optical characteristics of the image system, such as focal length, mirrors, etc. Finally we can apply the calibrated mapping functions to convert image pixel coordinates into azimuth and elevation angles.

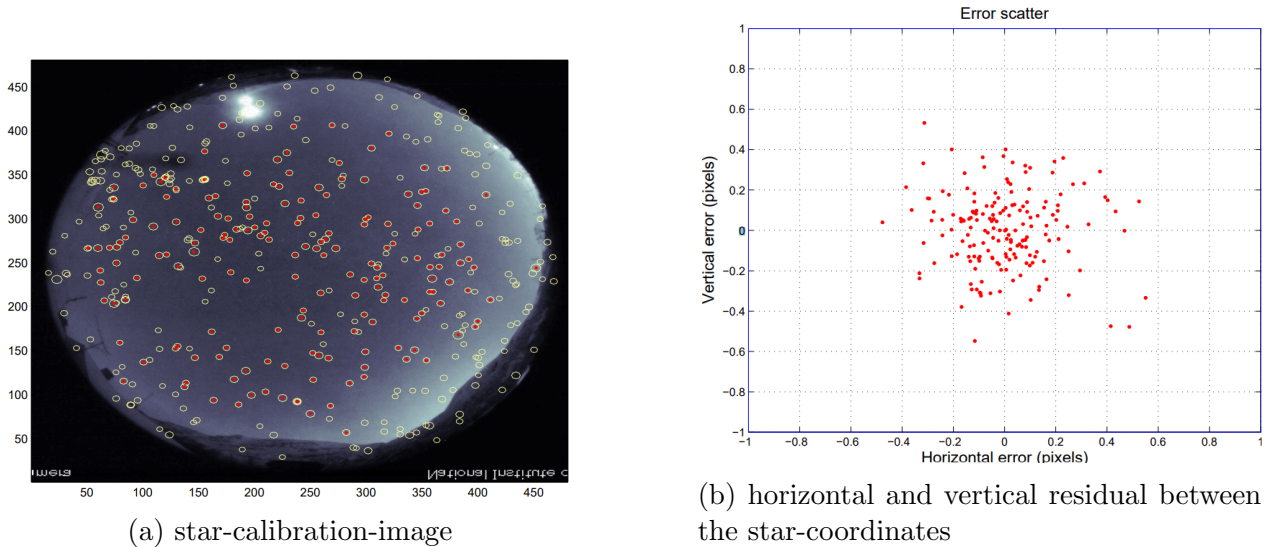


Figure 32

6.6 Calculating the unit vectors from two different auroral imagers

There is an example program for calculating the unit vectors from two different auroral imagers towards an artificial aurora blob created using the Tromsø ionospheric heating facility. Complete the program to determine the location of the centroid of the artificial aurora blob. This shouldn't be much more than 6 lines of additional code. The correct result is given in the final comments of the code. You'll find the mathematics in the lecture notes for triangulation.

<https://github.com/jvierine/fys3002/tree/main/optics>

To calculate for the stereoscopic triangulation, we use that.

$$\begin{aligned} r_2 \cdot e_1 - r_1 \cdot e_1 &= \ell_1 e_1 \cdot e_1 - \ell_2 e_2 \cdot e_1 \\ r_2 \cdot e_2 - r_1 \cdot e_2 &= \ell_1 e_1 \cdot e_2 - \ell_2 e_2 \cdot e_2 \end{aligned} \quad (41)$$

which looks like this in matrix form, with some modifications $A^{-1} \cdot m = x$.

$$\begin{bmatrix} 1 & e_2 \cdot e_1 \\ e_1 \cdot e_2 & -1 \end{bmatrix}^{-1} \cdot \begin{bmatrix} r_2 \cdot e_1 - r_1 \cdot e_1 \\ r_2 \cdot e_2 - r_1 \cdot e_2 \end{bmatrix} = \begin{bmatrix} \ell_1 \\ \ell_2 \end{bmatrix} \quad (42)$$

We complete the program, for calculating the location of the centroid of the artificial blob, by adding the following:

```
1 A = n.array([N_unit_vec[:2], -S_unit_vec[:2]]).T # Transpose to fit the
   shape (2, 2), matrix A^-1
2 delta_location = S_location[:2] - N_location[:2]
3 m = delta_location
```

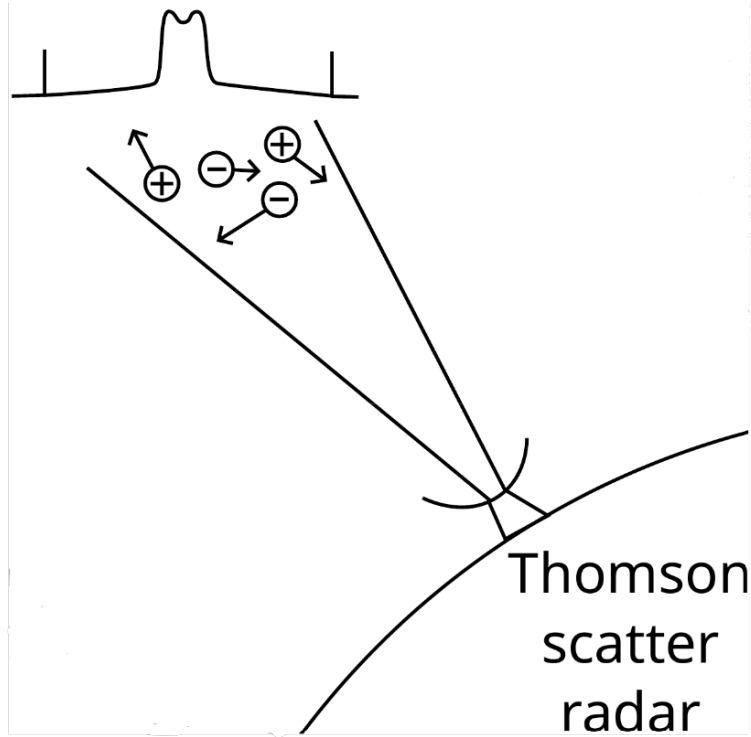
Listing 8: Added code using eq.38

This gives the following output.

```
Nikkaluokta blob position 69.27 N 19.18 E 236.39 km over sea level
Silkkimuokta blob position 69.27 N 19.18 E 236.47 km over sea level
```

Which correlates well with the approximations of the coordinates that were given.

7 Incoherent scatter radar exercises



7.1 Primary plasma parameters

The incoherent scatter radar technique is used to measure the ionosphere. What are the primary plasma parameters that can be measured with such a radar?

By using the incoherent scatter radar technique, we are able to measure the primary plasma parameters such as electron density (n_e), electron temperature (T_e), ion temperature (T_i) and ion velocity (v_i).

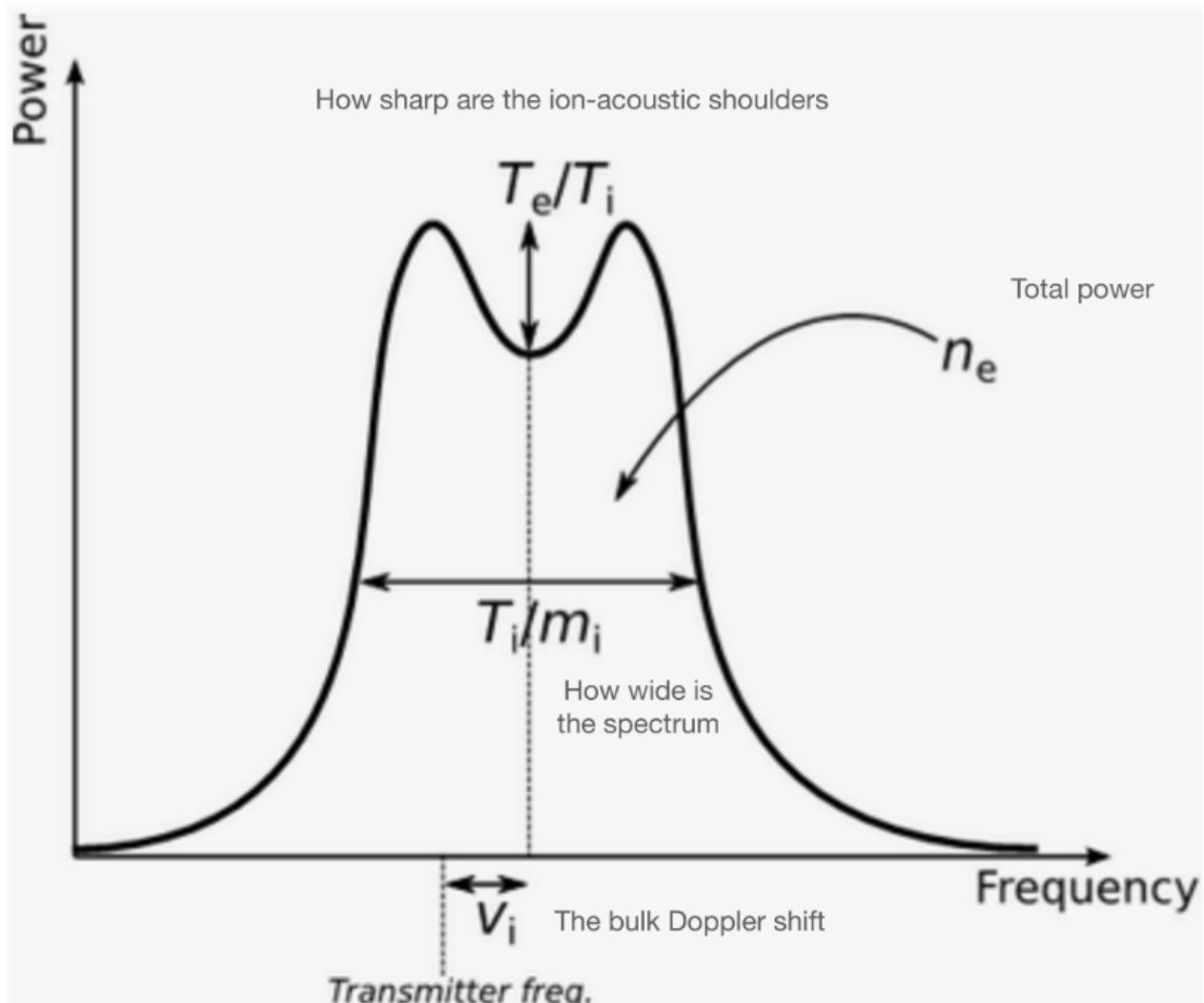


Figure 33: Ion-line features

7.2 The attribute "collective"

The incoherent scatter radar technique is also sometimes called the collective Thomson scatter radar technique. What physical phenomena does the attribute "collective" refer to?

The attribute "collective" refers to the scattering process, that involves a large number of charged particles collectively influencing the radar signal, as opposed to individual scattering events.

7.3 Calculate the radar cross-section

Radar systems with large antennae and powerful transmitters are needed to measure Thomson scatter from ionospheric electrons. Please calculate the radar cross-section of a 1 km³ volume

of ionospheric plasma that has an electron density of 10^{11} electrons per cubic meter. Assume a monostatic radar.

The radar cross-section is defined as.

$$\sigma_{tot} = V n_e \sigma_e \left(1 + \frac{T_e}{T_i}\right)^{-1} \quad (43)$$

Where V is the volume of the ionospheric plasma and σ_e is the electron cross-section ($9.98 \cdot 10^{-29} m^2$), for the correction factor containing T_e/T_i we will not consider it as to about 150km the electron- and ion-temperature is approximately the same. we can then compute it, and we get the following.

$$\sigma_{tot} = V n_e \sigma_e \quad (44)$$

$$= 1000 m^3 \cdot 10^{11} \cdot 9.98 \cdot 10^{-29} m^2 \quad (45)$$

$$= 9.98 \cdot 10^{-15} m^2 \quad (46)$$

Hence, we have a that the radar cross-section of a 1 km^3 of an ionospheric plasma is $9.98 \cdot 10^{-15} m^2$.

7.4 Calculate the ratio of received echo power and system noise power

Take the radar cross-section from the previous exercise and calculate the ratio of received echo power and system noise power (signal-to-noise ratio) for the EISCAT UHF radar. You can assume that the transmit power is 1 MW, the antenna gain is 48 dB, the radar frequency is 930 MHz, and that the system noise temperature is 100 K. The volume of plasma that you are measuring is at a distance of 200 km from the radar. Assume a monostatic radar.

For calculating the *received echo power*, we are given the following equation.

$$P_r = \frac{P_t G_t A_r V_s \sigma}{(4\pi)^2 R^4} \quad (47)$$

Where P_t is the power transmitted, G_t is the transmit antenna focus power (gain), A_r effective area of the receiving antenna, R distance between the target is from the radar, σ is our radar cross-section and V_s scattering volume from the previous task. We can define A_r as.

$$A_r = \frac{G_t \lambda^2}{4\pi} = \frac{10^{4.8} \cdot 0.32^2}{4\pi} = 514.15 m^2 \quad (48)$$

Then we can calculate the received power.

$$P_r = \frac{10^6 W \cdot 10^{4.8} \cdot 514.15 m^2 \cdot 1000 m^3 \cdot 9.98 \cdot 10^{-15} m^2}{(4\pi)^2 (200 \cdot 10^3 m)^4} \quad (49)$$

$$= \underline{\underline{1.28 \cdot 10^{-21} W}} \quad (50)$$

The received echo power is $1.28 \cdot 10^{-21}W$. For calculating the *system noise power* (signal-to-noise ratio), we are using the following formula.

$$\frac{P_r}{N} = \frac{P_t c T_p \sigma A_e \lambda}{8\pi R^2 k T_{sys} w_{IL}} \quad (51)$$

where N is the Johnson-Nyquist noise model, which we can compute as.

$$N = k_b T B = 1.38 \cdot 10^{-23} J K^{-1} \cdot 100 K \cdot 930 \cdot 10^6 Hz = \underline{\underline{1.28 \cdot 10^{-12} W}} \quad (52)$$

This means that we have a signal-to-noise ratio (SNR) of.

$$SNR = \frac{P_r}{N} = \frac{1.28 \cdot 10^{-21} W}{1.28 \cdot 10^{-12} W} = \underline{\underline{1.0 \cdot 10^{-9}}} \quad (53)$$

Hence, the ratio of received echo power and system noise power (signal-to-noise ratio) is $1.0 \cdot 10^{-9}$.

7.5 sketch the ion-line feature and explain the plasma parameters

Please sketch the ion-line feature of the incoherent scatter radar Doppler spectrum. Explain how the following plasma parameters affect the shape of the ion-line T_e/T_i , n_e , T_i , m_i .

We have the following plasma parameters which affect the shape of the ion-line T_e/T_i , n_e , T_i , and m_i . A good illustration of a sketch of the ion-line, can be seen in figure 33

The electron temperature (T_e) to ion temperature (T_i) ratio (T_e/T_i), tends to broaden the ion line between the shoulder peaks. This happens because higher electron temperature increases the random motion of electrons, which increases the collision frequency between electrons and ions. These collisions lead to a broader Doppler spectrum for ion scattering. If we have an increase in electron density (n_e), we often get a stronger ion line. This comes from the fact that a higher electron density provides more scattering targets for the radar waves, leading to a stronger ion line.

An enhanced ion temperature (T_i) has similar effects as the T_e/T_i ratio, it will broaden the ion-line. Higher T_i leads to increased ion velocity and collision frequency, resulting in a broader Doppler spectrum.

At last, we have the ion mass (m_i), which doesn't give as strong an impact as the other parameters. But, heavier ions tend to produce a broader ion line due to their slow thermal velocities. Hence, the ion mass and temperature is perfectly correlated.

7.6 Optimal incoherent scatter radar frequency and performance degrade

It is possible to find an optimal incoherent scatter radar frequency by inspecting signal-to-noise power ratio of the ion-line spectrum as a function of radar frequency. Explain what is

an optimal frequency to use for incoherent scatter radar. Why does performance degrade for frequencies below the optimum? Why does performance degrade above this optimum?

For finding the optimal frequency, we commonly examine the signal-to-noise power ratio (SNR) of the ion line spectrum as a function of the radar frequency. The *optimal frequency* for ISR typically lies within a certain range. *Performance degradation* occurs for frequencies below and above the optimum due to different factors. **Below optimum frequency**, the radar waves penetrate deeper into the ionosphere before scattering back. This deeper penetration reduces the effective scattering volume and results in weaker signals received. We can also have the ionospheric plasma frequency that exceeds the radar frequency, and we get a cutoff. **Above optimum frequency** the radar waves are less efficiently scattered by the free electrons in the ionosphere. This leads to weaker return signals and reduced SNR. At a higher frequency, the waves can experience more absorption by neutral atmospheric components.

7.7 Three examples of other uses for these large radars

Powerful incoherent scatter radar systems can also be used for purposes beyond studies of ionospheric plasma parameters. Provide three examples of other uses for these large radars (and radio telescopes).

Three examples of other uses for these large radars (and radio telescopes), are planetary radar astronomy, atmospheric dynamics and space weather, and ionospheric experiments.

7.7.1 Planetary Radar Astronomy

Incoherent scatter radar systems, when equipped with high-power transmitters and sensitive receivers, can serve as a powerful tool for planetary radar astronomy. By transmitting radio pulses toward nearby planets and asteroids and analyzing the echoes returned from their surfaces and atmospheres, this gives insight into the planetary surface features and orbital dynamics, etc. Figure 34 illustrates this. (e.g. the Arecibo telescope)

7.7.2 Atmospheric dynamics and space weather

We can also use incoherent scatter radars to study the dynamics of the upper atmosphere. By observing how radio waves interact with charged particles and neutral gases, we can investigate phenomena such as atmospheric tides, gravity waves (which was done with the Arecibo telescope), and variations in electron density, etc.

7.7.3 Ionospheric experiments

We can also conduct ionospheric modification experiments, by transmitting high-power radio waves into the ionosphere, this allows for controlled changes in the electron density and temperature, creating artificial plasma disturbances.

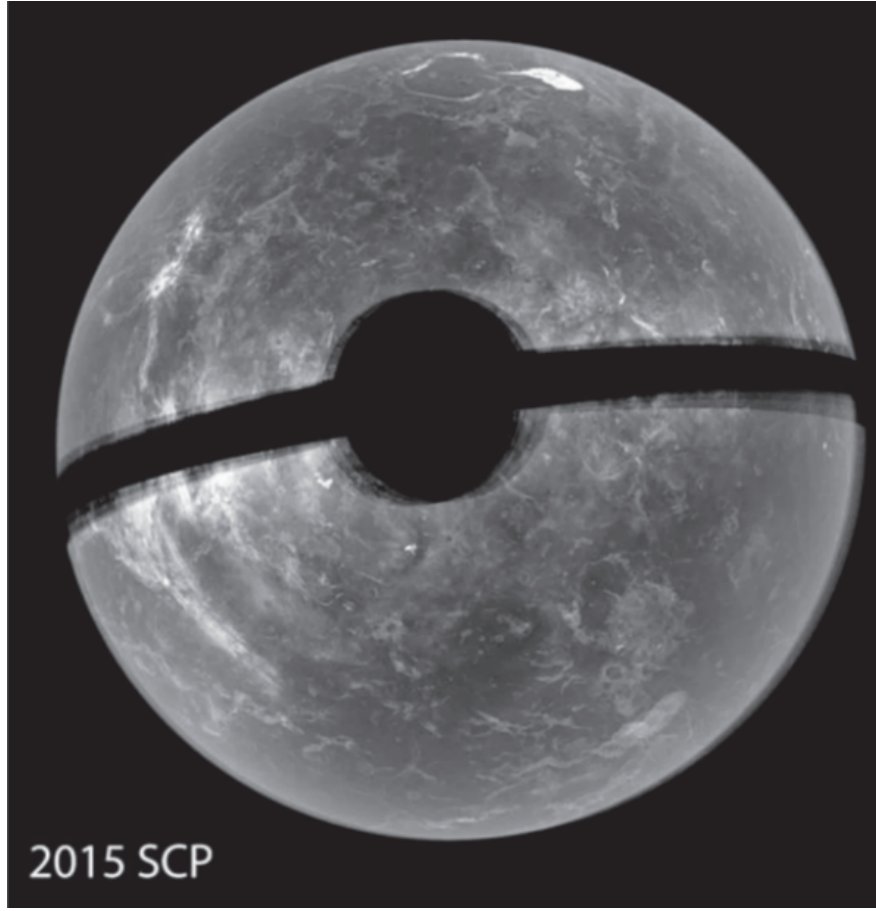


Figure 34: figure from the lecture notes, Arecibo telescope

7.8 The magic constant γ

Electron density can be determined from the amount of power contained within the ion-line measured with an incoherent scatter radar. One complication that radar systems often face is that the antenna effective area is poorly known, and it can also change from day-to-day due to e.g., snow deforming the antenna dish. Explain the procedure for estimating the magic constant that allows calibrating an incoherent scatter radar measurement. The magic constant includes the antenna effective area. What measurements can be used to determine the magic constant?

The magic constant γ is defined as:

$$\gamma = \frac{P_t c T_p \sigma_e A_{BS}}{8\pi k_b B} \quad (54)$$

Where P_t is the transmitter power, c is the speed of light, T_p is the radar pulse length, A_{BS} is the effective antenna aperture size, σ is the radar cross-section and B is the bandwidth. The power received by the radar system depends on different factors, which include the radar

cross-section of the target (e.g. ionosphere), the radar transmit power, and the characteristics of the receiving antenna. By comparing the received power with a known standard or calibration source, it is possible to determine the magic constant that relates the received power to the actual electron density in the ionosphere. One of the measurements that can be used to determine the magic constant is antenna gain measurements, which involves directly measuring the gain pattern and effective area of the radar antenna this can be done through antenna scans. By characterizing the antenna's performance under various conditions (e.g. snow deforming the antenna dish) we can estimate how changes in the antenna's effective area affect the received power. Another measurement method is to use independent measurements from other instruments such as ionosonds that can provide measurements of electron density, allowing for cross-validation an example of this is shown in figure 35. It can also be possible to use noise injection.

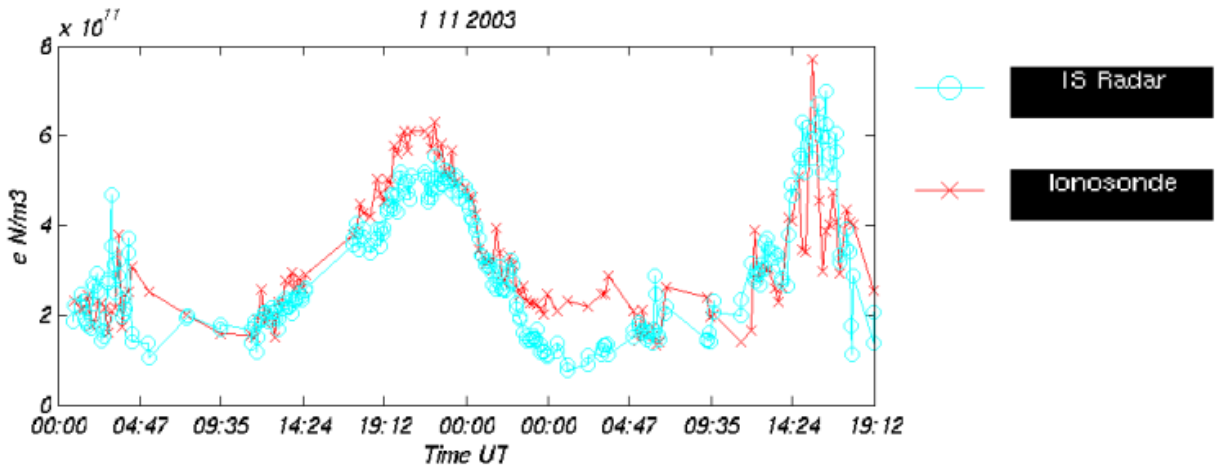


Figure 35: Figure from: Calibration of EISCAT incoherent scatter radar electron densities and the anomaly of 23-25 October 2003

7.9 Range-time diagram to describe where in range-time space the radar scatter originates from

The pulse length of a radar system influences where in range and time signals scatter from. Assume that the transmit pulse is $T_p = 30\mu s$ and the receiver impulse response is a boxcar function of length $T_p = 30\mu s$. Draw a range-time diagram to describe where in rangetime space the radar scatter originates from. Assume a $\Delta t = 1ms$ is the spacing between the leading edge of the transmit pulse and the leading edge of the receiver sample.

Figure 36 shows the range-time diagram.

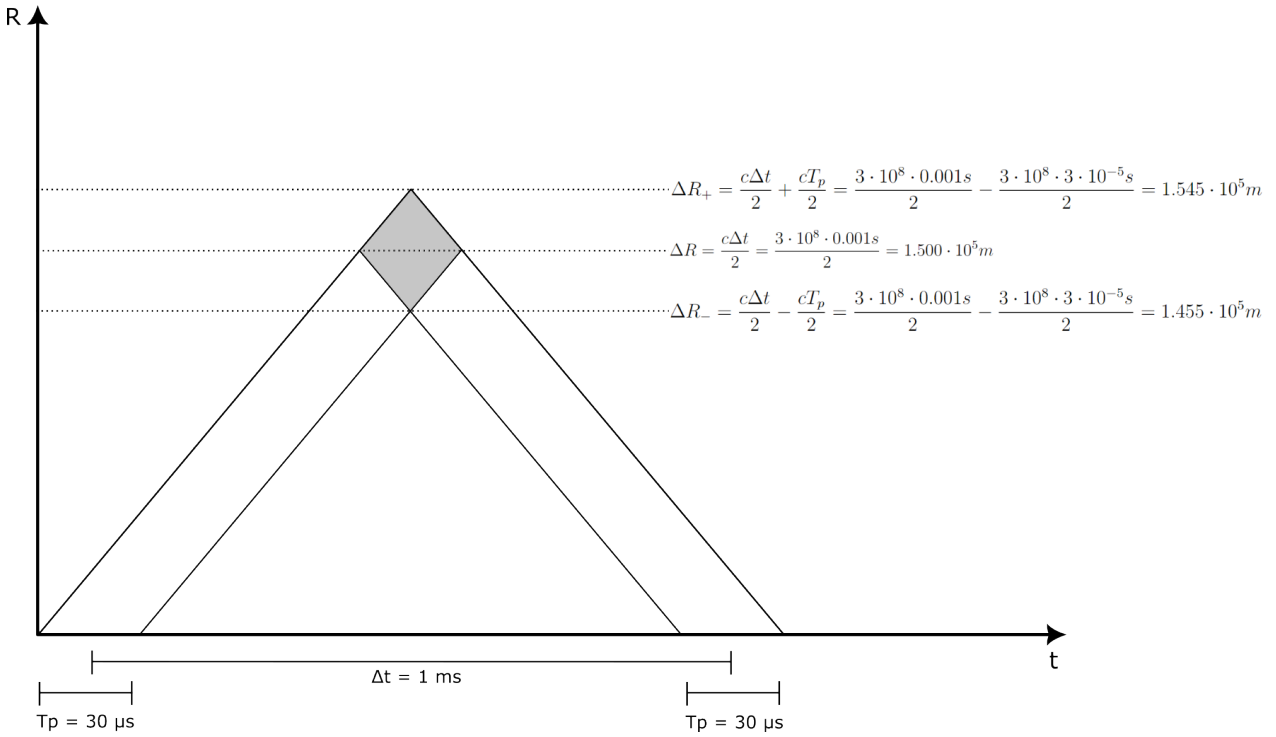


Figure 36: Range-time diagram, (Trym Varland, 2024)

From the calculations down below, we see that radar scatter originates from a space between $1.455 \cdot 10^5 m$ and $1.545 \cdot 10^5 m$.

$$\Delta R_+ = \frac{c\Delta t}{2} + \frac{cT_p}{2} = \frac{3 \cdot 10^8 \cdot 0.001s}{2} + \frac{3 \cdot 10^8 \cdot 30 \cdot 10^{-6}s}{2} = 1.545 \cdot 10^5 m$$

$$\Delta R = \frac{c\Delta t}{2} = \frac{3 \cdot 10^8 \cdot 0.001s}{2} = 1.500 \cdot 10^5 m$$

$$\Delta R_- = \frac{c\Delta t}{2} - \frac{cT_p}{2} = \frac{3 \cdot 10^8 \cdot 0.001s}{2} - \frac{3 \cdot 10^8 \cdot 30 \cdot 10^{-6}s}{2} = 1.455 \cdot 10^5 m$$

The scattered area is about, 9000m thick. Further we can use this to calculate the scattering volume.

7.10 Plasma-parameters

What plasma-parameter can the plasma-line be used to measure?

The plasma line in incoherent scatter radar measurements refers to a characteristic feature in the radar spectrum caused by scattering from free electrons in the ionosphere. This plasma line can be used to measure the electron density (n_e), electron temperature (T_e), and electron velocity (v_e) of the ionosphere. But calculating for the electron temperature and velocity is

very hard. The first term in eq.50 gives rise to the plasma line (electron line term), which is driven by electron thermal fluctuation.

$$\langle |n_e(k, \omega)|^2 \rangle = \frac{|j\omega\epsilon_o + \sigma_i|^2 \langle |n_{te}(k, \omega)|^2 \rangle}{|j\omega\epsilon_o + \sigma_e + \sigma_i|^2} + \frac{|\sigma_e|^2 \langle |n_{yi}(k, \omega)|^2 \rangle}{|j\omega\epsilon_o + \sigma_e + \sigma_i|^2} \quad (55)$$

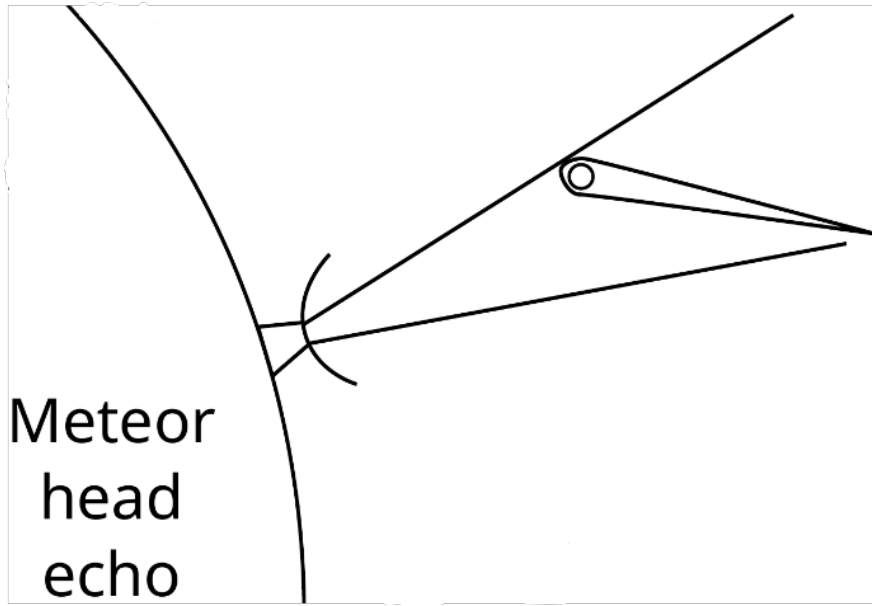
Here $n_{te}(\mathbf{k}, \omega)$ is the thermally driven electron contribution to current, $n_{ti}(\mathbf{k}, \omega)$ is the thermally driven ion contribution to current, σ_e is electron admittance, σ_i is ion admittance, and the term $j\omega\epsilon_o$ is the capacitance of free space.

7.11 Scattered power reduced proportionally to $1/R^2$

For a mono-static radar, the radar equation states that the amount of power from a radar target reduces as a function of range proportionally to $1/R^4$. In the case of incoherent scatter from ionospheric plasma, the scattered power is only reduced proportionally to $1/R^2$. Explain why.

As the target is volume filling, radar back-scattered power decreases in range proportional to $1/R^2$. Incoherent scatter radar works by transmitting radio waves into the ionosphere, where they interact with free electrons. These electrons scatter the incident waves in all directions. The scattered waves, which are essentially radiated by the electrons, spread out in all directions, including back toward the radar receiver. In contrast to a radar target, where the received power decreases rapidly with range due to geometric spreading and attenuation, the scattering from ionospheric plasma follows a simpler attenuation pattern, resulting in a decrease proportional to $1/R^2$ rather than $1/R^4$.

8 Meteor head echo exercises



8.1 Meteor head echo

What is a meteor head echo? How does it differ from the meteor trail echo? What parameters can be estimated from a meteor head echo?

The meteor head echo is a radar echo from the dense cloud of plasma moving at unison with the ablating meteor. As for the meteor trail echo, that is a coherent echo from the plasma suspended in the atmosphere behind the ablating meteor. From the meteor head echo we can estimate the velocity of the meteoroid, the trajectory, size, mass, and the atmospheric density.

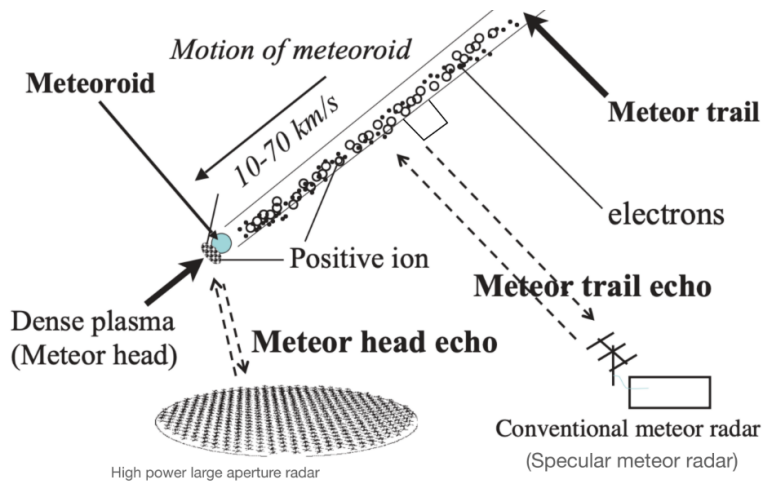


Figure 37: Meteor head echo lecture, page.6

8.2 Radar cross-section of a meteor head

The radar cross-section of a meteor head echo is radar frequency dependent. Explain why. Does the radar cross-section of a meteor head echo increase with increasing radar frequency?

The radar cross-section of a meteor head echo is radar frequency dependent. One of the reasons is that the radar cross-section of a meteor head echo is influenced by the size of the meteoroid and its interaction with radar waves. Larger meteoroids tend to have larger radar cross-section values because they present a larger target for the radar waves to interact with. Also when the size of the target is similar to the wavelength of the radar waves, a resonance effect can occur which increases the scattering and the radar cross-section. At higher frequencies, the meteoroid size may become more comparable to the wavelength of the radar waves. This can lead to resonance effects that lead to increased radar cross-section compared with lower frequencies. We also have the scattering mechanisms involved in producing a meteor head echo can vary with radar frequency. At lower frequencies, mechanisms such as geometric scattering and diffraction dominate, while at higher frequencies, effects such as **Mie** scattering become more prominent, as shown in figure

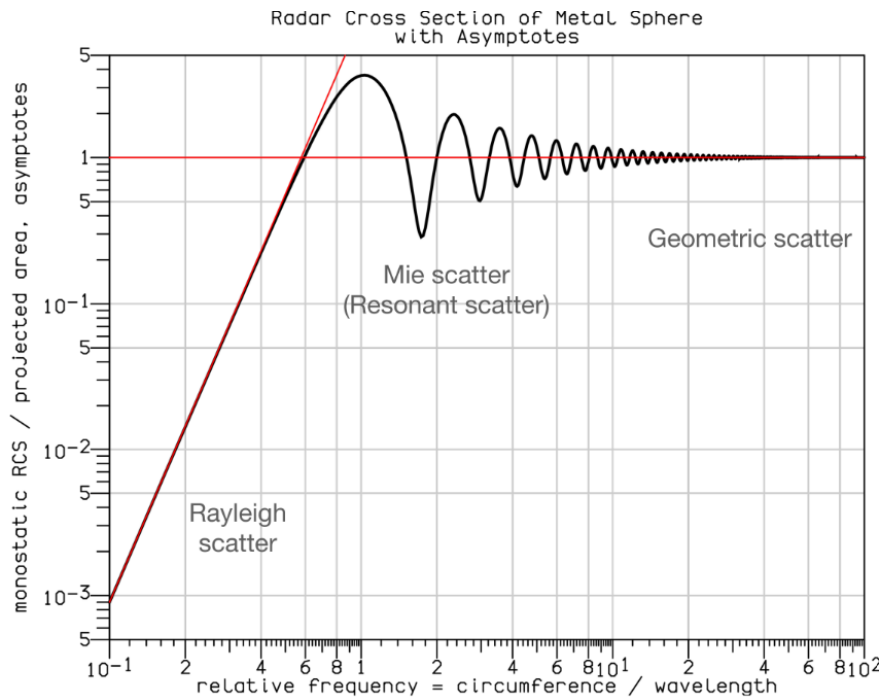


Figure 38: The classical radar cross-section of perfectly conducting sphere is a good approximation for the meteor head echo radar cross-section. [lecture notes]

8.3 Estimating meteoroid mass

What are the two primary methods for estimating meteoroid mass using meteor head echos?

Two methods can be used for estimating the meteoroid mass using meteor head echos, that is the *radar cross-section mass* and the *dynamic mass*.

Radar cross-section mass is based on radar cross-section is proportional to the ablation rate (mass-loss rate).

Dynamic mass is based on the deceleration of an object affected by drag being related to area to the to-mass ratio. By assuming an area-to-mass ratio and measuring the velocity and deceleration, it is possible to estimate mass.

Radar-cross-section mass	Dynamic mass
$m = \int_{t_0}^{t_1} \frac{qU\mu}{\beta} dt$	$m_d = -\frac{15}{4\rho_m^2} \left(\frac{\rho_a v^2}{2\partial_t v} \right)^3$

(56)

8.4 Derive the Halliday equation and assumptions

Derive the Halliday equation for dynamic mass of a meteoroid entering the Earth's atmosphere:

$$m_d = -\frac{15}{4\rho_m^2} \left(\frac{\rho_a v^2}{2\partial_t v} \right)^3 \quad (57)$$

Here ρ_m is the meteoroid density, ρ_a is atmospheric density, v is the absolute velocity, and a is the acceleration due to atmospheric drag. What prior assumptions need to be made in order to estimate meteoroid mass? What happens if your assumption of meteoroid density wrong by a factor of 10?

As the meteoroid has its atmospheric entry, we have a dominant atmospheric drag. Så by using Newton's second law, we can express drag force as.

$$F_d = m \cdot a \quad (58)$$

where m is the mass of the meteoroid and a is the acceleration due to atmospheric drag. The acceleration a can be related to velocity v and the atmospheric density ρ_a , as.

$$a = \frac{1}{2} C_d \rho_a S v^2 \quad (59)$$

Here C_d is the drag coefficient and S is the cross-sectional area of the meteoroid. The dynamic mass of the meteoroid is defined as the effective mass of the meteoroid experiencing the declaration of forces of atmospheric drag, hence we can express it as.

$$m_d = \frac{F_d}{a} \quad (60)$$

Substituting the expressions for F_d and a we get.

$$m_d = \frac{m}{\frac{1}{2} C_d \rho_a S v^2} = \frac{2m}{C_d \rho_a S v^2} \quad (61)$$

As the shape of the object is assumed to be brick-like with side lengths $2L$, $3L$ and $5L$. We have $S = 15L^2$, and $m_d = 30\rho_m L^3$ here ρ_m is the density of the meteoroid. We can then obtain the Halliday equation for dynamic mass by substituting the dynamic mass eq into the drag force equation and rearranging terms, it takes the form.

$$m_d = -\frac{15}{4\rho_m^2} \left(\frac{\rho_a v^2}{2\partial_t v} \right)^3 \quad (62)$$

We have also made the assumption that $C_d = 1$.

If the assumption of the meteoroid density is wrong by a factor of 10, it would significantly affect the estimation of the dynamic mass. A high estimation of the meteoroid density leads to underestimating the dynamic mass, and vice-versa.

8.5 Interferometry and tri-static observation of trajectory

The trajectory of a meteor can be estimated with two different methods from meteor head echoes using a powerful radar system: 1) with interferometry, or 2) using a tri-static observation. Explain how these two methods work.

Tri-static observation uses geometry, and three independent delays (transmitter-receiver) as we will get three independent Doppler shifts. Unambiguously determines the three-dimensional path and vector velocity of the meteor.

interferometry means we can use one single radar for the meteor trajectory estimations. Comparing the phases (arrival time) of the incoming plane wave at each section of the antenna, the angle of arrival of the plane wave can be determined. By measuring the delay between the transmit and reception of radar echo, the range can be estimated. By combining angle and distance measurement, a 3D position can be determined.

8.6 Determine the velocity and acceleration of the meteor (MAARSY)

There is an example meteor head echo event from the MAARSY radar on github: https://github.com/jvierine/fys3002/tree/main/meteor_head The example program `example_read_event.py` reads the time, position, and signal-to-noise ratio of the meteor head echo. Determine the velocity and acceleration of the meteor. You can e.g., fit a polynomial trajectory model independently for the east-west, north-south, and up-down positions:

$$p_x(t) = p_x + v_x t + \frac{1}{2} a_x t^2 \quad (63)$$

where $p_x(t)$ is the x -component of the position as a function of time, which is either east-west, north-south, or up-down. This results in a linear least squares problem:

$$\begin{bmatrix} x_1 \\ x_2 \\ \vdots \\ x_N \end{bmatrix} = \begin{bmatrix} 1 & t_1 & \frac{1}{2}t_1^2 \\ 1 & t_2 & \frac{1}{2}t_2^2 \\ \vdots & \vdots & \vdots \\ 1 & t_N & \frac{1}{2}t_N^2 \end{bmatrix} \begin{bmatrix} p_x \\ v_x \\ a_x \end{bmatrix}$$

Here x_i is the i th measurement of coordinate x , t_i is the time of the i th measurement, p_x is the initial position at $t = 0$, v_x is the initial velocity at $t = 0$, and a_x is the acceleration. The matrix equation can be solved in Python with `numpy.linalg.lstsq`. Alternatively, you can also fit a non-linear trajectory model to the measurements. Using the velocity and acceleration, determine the dynamic mass. You can assume that $\rho_m = 1000\text{kg/m}^3$ and $\rho_a = 1.4 \cdot 10^{-6}\text{kg/m}^{-3}$.

By using the time and the position, we end up with a linear least squares problem for the x-position, x-velocity, x-acceleration, y-position, and etc. Here we end up, with the following values for velocity and acceleration.

Velocity (east-west): $v_x = -41876\text{m/s}$	Acceleration (east-west): $a_x = 6438\text{m/s}^2$
Velocity (north-south): $v_y = 6761\text{m/s}$	Acceleration (north-south): $a_y = -7520\text{m/s}^2$
Velocity (up-down): $v_z = -34615\text{m/s}$	Acceleration (up-down): $a_z = 17262\text{m/s}^2$

Than the average velocity and acceleration of the meteor are.

Velocity: 54.8km/s	Acceleration: 19.9km/s^2
-----------------------------	-----------------------------------

at the end we get that the dynamic mass of the meteor is:

$$m_d = -\frac{15}{4\rho_m^2} \left(\frac{\rho_a(\sqrt{v_x^2 + v_y^2 + v_z^2})^2}{2\sqrt{a_x^2 + a_y^2 + a_z^2}} \right)^3 = -4.3 \cdot 10^{-9}\text{kg} \quad (64)$$

```

1 def fit_trajectory_model(time, pos):
2     # assuming initial velocity and acceleration are zero,
3     # maybe use "initial_velocity*time + 0.5*acceleration*time^2" model
4     A = np.vstack([np.ones(len(time)), time, 0.5*time**2]).T # matrix A
5     coefficients, _, _, _ = lstsq(A, pos, rcond=None) # least squares
6     solution to A*x = pos
7     return coefficients
8
9
10
11
12
13
14
15
16
```

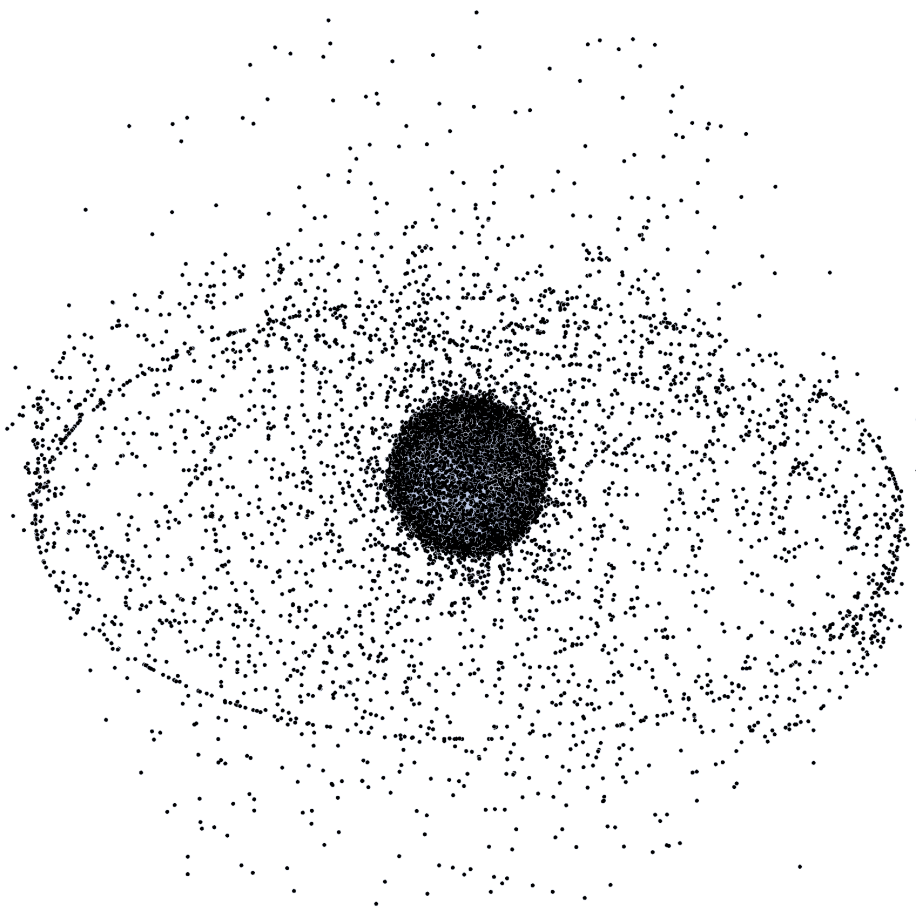
```

17 az = 2 * coefficients_up_down[2] # acceleration up-down
18
19 a_avg = np.sqrt(ax**2 + ay**2 + az**2)
20 print("Average Acceleration:", a_avg, "m/s^2")
21 v_avg = np.sqrt(vx**2 + vy**2 + vz**2)
22 print("Average Velocity:", v_avg, "m/s")
23
24 dynamic_mass = - 15/(4*rho_m**2) * (rho_a*(v_avg)**2/(2*np.sqrt(ax**2 + ay
    **2 + az**2)))**3
25
26 print("Velocity (east-west):", vx, "m/s")
27 print("Acceleration (east-west):", ax, "m/s^2")
28 print("Velocity (north-south):", vy, "m/s")
29 print("Acceleration (north-south):", ay, "m/s^2")
30 print("Velocity (up-down):", vz, "m/s")
31 print("Acceleration (up-down):", az, "m/s^2")
32 print("Dynamic Mass:", dynamic_mass, "kg")

```

Listing 9: Code for determine the velocity and acceleration of the meteor from the MAARSY radar

9 Space debris exercises



9.1 Kessler syndrome

What is the Kessler syndrome? For extra credit, propose a solution to solve it.

The Kessler syndrome, is a theoretical scenario proposed by Donald J. Kessler in 1978. It describes a scenario in low Earth orbit (LEO) where the density of objects, as defunct satellites, rocket stages and other debris, is high enough that collisions between objects could cause a cascade of further collisions. This cascade would generate a significant increase in debris, leading to a further increase in collision risk and making space activities in LEO increasingly hazardous.

One solution for this would be active debris removal, which includes actively removing existing debris from orbit using spacecraft with robotic arms, nets, or other capture mechanisms. These spacecraft could capture the debris, and deorbit them or move them to safer orbits. Another solution, which is ongoing now is having more strict rules for how long a satellite can orbit and then re-enter the atmosphere by itself.

9.2 parameters to obtain information about the properties of the space debris objects

Beam park radar measurements of space debris can be used to study the evolution of space debris. The radar measures time, range, Doppler shift, and signal-to-noise ratio for objects randomly passing the radar beam. Assume that the radar is pointing 15 degrees East of zenith. How can you use these parameters to obtain information about the properties of the space debris objects, including object size, inclination, longitude of the ascending node, and semi-major axis. You can assume the objects to be on circular orbits.

To obtain information about the properties of the space debris such as size, inclination, longitude of the ascending node, and the semi-major axis.

By using the time and range measurements we can find out the position of the object relative to the radar. By tracking the object over time, we can determine its orbit and calculate parameters such as **semi-major axis** and eccentricity.

The relative motion between the radar and the object causes the Doppler shift observed in the retrieved signal. The magnitude and direction of the Doppler shift can give information about the object's radial velocity, which combined with range rate information, can be used to determine the object's orbit parameters.

The signal-to-noise ratio provides information about the strength of the radar return signal compared with background noise. Higher SNR values indicate a stronger signal return, which can be associated with larger objects. This can also be used to estimate the density of objects in Earth orbit, this is something they do at the radar Beam park.

By using these parameters/measurement methods. So for the orbit determination, we use time, range, and Doppler shift measurements to determine the orbital parameters, such as **semi-major axis**, **eccentricity**, and **inclination**. This can be done by using sequential estimation methods for example. By using signal-to-noise measurement, we can find information about the **object's size or surface**. Larger or more reflective objects produce stronger radar returns, giving rise to higher SNR values. Once the object orbit is determined, its **inclination** and **longitude of the ascending node** can be derived from the orbital elements.

9.3 relate antenna gain G and antenna effective area A_{eff}

For a circular radio antenna, one can relate antenna gain G and antenna effective area A_{eff} to one another. How are they related?

The relationship between effective area and gain:

$$A_{eff} = \frac{G\lambda^2}{4\pi} \quad (65)$$

Where λ is the wavelength of the radio waves. The *effective area* of the antenna is a measure of its ability to capture power from or radiate power into space. It is essentially the cross-sectional area of the antenna as "seen" by the incoming or outgoing electromagnetic waves.

The *antenna gain* describes how much the antenna concentrates the power radiated in a particular direction compared to an isotropic radio. So, a large effective area generally leads to a higher gain, indicating that the antenna is more directive in its radiation pattern and can capture or emit more power in the desired direction.

9.4 Diameter much smaller than the wavelength

It is difficult for radars to detect space debris objects that have a diameter much smaller than the wavelength. Why is this?

When the diameter of the space debris object is much smaller than the wavelength of the radar signal, it becomes difficult for the radar to detect these objects due to the Rayleigh scattering. In this Rayleigh regime, the scattered radiation is proportional to the fourth power of the ratio of the object's size to the wavelength (seen in eq.66 as part of the radar equation for received power eq.47). When the size of the space debris object is much smaller than the wavelength, the scattering efficiency is very low. This means that only a small fraction of the incident radar signal is scattered back toward the radar receiver, making the object's radar cross-section small. The small radar cross-section results in a weaker radar return, which can easily be overwhelmed by noise or other background signals.

$$\frac{\sigma_*}{\frac{1}{4}\pi d^2} = \begin{cases} 9\left(\frac{\pi d}{\lambda}\right)^4 & , \text{ when } d < \frac{\lambda}{\pi\sqrt{3}} \\ 1 & , \text{ when } d > \frac{\lambda}{\pi\sqrt{3}} \end{cases} \quad (66)$$

9.5 Signal-to-noise ratio for a 0.1 m diameter cubesat

The radar equation

$$P_{rec} = \frac{P_t G \sigma_* A_{eff}}{(4\pi)^2 R^2} \quad (67)$$

and the Johnson-Nyquist noise formula

$$P_{noise} = k_b T_{sys} B \quad (68)$$

can be used to calculate the signal-to-noise ratio of satellites and space debris. Here P_{rec} is the power received by a radar system, P_t is the transmitted power, G is antenna gain, A_{eff} is the effective area of the radar antenna, σ_ is the radar cross-section of the object, P_{noise} is the amount of receiver noise, k_B is the Boltzmann constant, T_{sys} is the system noise temperature, and B is the receiver noise bandwidth. Assuming that the radar range-velocity-acceleration matched receiver filter length used to detect satellites is $\tau = 0.02$ seconds long, the receiver bandwidth, based on the time-frequency uncertainty principle of signal processing, is $B = \tau^{-1} = 50$ Hz. What is the signal-to-noise ratio for a 0.1 m diameter 1 U cubesat at 500 km distance when using a 930 MHz radar system, which has system noise temperature $T_{sys} = 100K$, and $P_t = 106W$, and $G = 10^{4.8}$? You can assume that the 1 U cubesat is a*

metallic sphere with a diameter of 0.1 m.

We know that the signal-to-noise ratio is given by.

$$SNR = \frac{P_{rec}}{P_{noise}} \quad (69)$$

We start by calculating P_{noise} as.

$$P_{noise} = k_b T_{sys} B = (1.38 \cdot 10^{-23} J/K) \cdot 100K \cdot 50Hz = 6.9 \cdot 10^{-20} W \quad (70)$$

Now for calculating the power received by the radar system (P_{rec}), we need to calculate the A_{eff} and σ_* . So for the effective area of the radar antenna, we obtain.

$$A_{eff} = \frac{G\lambda^2}{4\pi} = \frac{10^{4.8} \cdot 0.323^2}{4\pi} = 523.836 m^2 \quad (71)$$

Then we can calculate the radar cross-section of the 1U cubesat.

$$\sigma_* = \pi D^4 = \pi(0.1)^4 = 3.14159 \cdot 10^{-4} m^2 \quad (72)$$

Finally, we can calculate the power received by the radar system.

$$P_{rec} = \frac{P_t G \sigma_* A_{eff}}{(4\pi)^2 R^2} = \frac{10^6 \cdot 10^{4.8} \cdot 3.14159 \cdot 10^{-4} \cdot 523.836}{(4\pi)^2 \cdot (500 \cdot 10^3)^4} = 3.305 \cdot 10^{-19} W \quad (73)$$

This gives that we have a signal-to-noise ratio of.

$$SNR = \frac{P_{rec}}{P_{noise}} = \frac{3.305 \cdot 10^{-19}}{6.9 \cdot 10^{-20}} = \underline{\underline{4.789}} \quad (74)$$

Therefore, the signal-to-noise ratio for the 0.1m diameter 1U cubesat at 500km distance using radar system parameters is approximately 4.789.

9.6 Furthest distance that you can observe the cubesat

Assume that you have a radar with $A_{eff} = 5m^2$ and $P_t = 103W$. Otherwise the radar parameters are the same as in the previous task. What is the furthest distance that you can observe the 0.1 m cubesat with $P_{rec}/P_{noise} > 10$?

For computing what the furthest distance is, which is where we can observe the 0.1m cubesat with $P_{rec}/P_{noise} > 10$. We need to solve for R, which comes from P_{rec} :

$$\frac{P_{rec}}{P_{noise}} > 10 \quad (75)$$

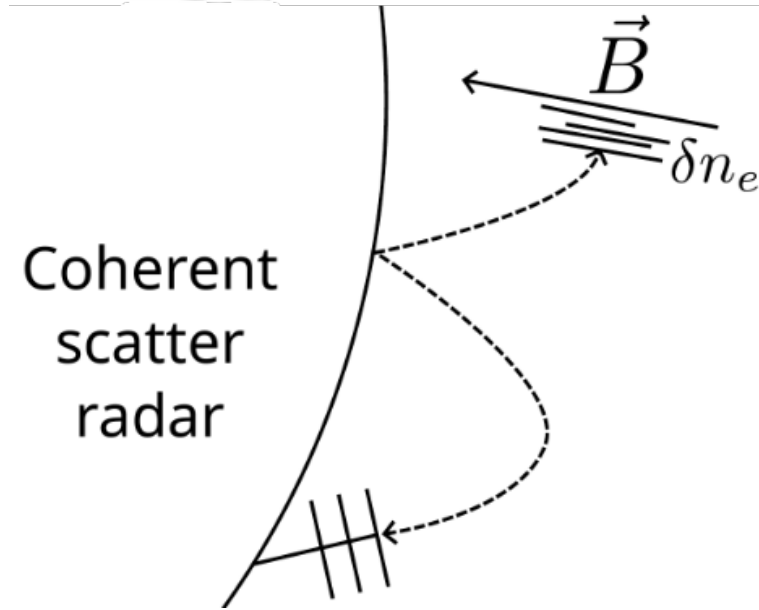
$$\frac{P_t G \sigma_* A_{eff}}{(4\pi)^2 R^2} > 10 \quad (76)$$

After some rearranging, we end up with.

$$R < \left(\frac{P_t G \sigma_* A_{eff}}{(4\pi)^2 \cdot k_B T_{sys} B \cdot 10} \right)^{\frac{1}{4}} \quad (77)$$

By using python for computation, the furthest distance that we can observe the cubesat with $P_{rec}/P_{noise} > 10$ is **173.67km**. This makes sense, as we will have a higher noise level the cubesat will need to be closer for us to separate it from the noise or to detect it at all.

10 Coherent scatter exercises



10.1 The SuperDARN over-the-horizon radar network observes the F-region (gradient drift instability mechanism)

The SuperDARN over-the-horizon radar network observes coherent scatter radar echoes from F-region ionospheric irregularities, which are primarily thought to be created by the gradient drift instability mechanism.

10.1.1 Snell's law, ray paths of radio waves, Appleton-Hartree equation

Use Snell's law, a typical ionospheric electron density altitude profile, and the Appleton-Hartree equation

$$n \approx \left(1 - \frac{f_p^2}{f_r^2}\right)^{-1/2}$$

to explain what causes the ray paths of radio waves used by SuperDARN to bend when they propagate through the ionosphere and make ionospheric radar observations from below the horizon. What are the terms n , f_r and f_p in the unmagnetized collisionless Appleton-Hartree equation shown above?

The *Snell's law* describes the change in direction of waves as they pass through different media with varying densities. In the context of the ionosphere and SuperDARN radar observation, Snell's law explains the bending of radio waves when they propagate through the ionosphere. As radio waves encounter regions of varying electron density within the ionosphere, they experience changes in their path due to the change in the refractive index of the

medium. The ionospheric density altitude profile refers to the distribution of electron density with altitude within the ionosphere. This profile typically shows an increase in electron density with increasing altitude up to certain point, followed by a decrease. The Appleton-Hartree equation provides an approximation for the refractive index n of the ionosphere, which influences the bending of radio waves. The equation is given by.

$$n \approx \sqrt{1 - \frac{f_p^2}{f_r^2}} = \sqrt{1 - \frac{\omega_p^2}{\omega^2}} = \sqrt{1 - \frac{n_e e^2}{\epsilon_0 m_e \omega^2}} \quad (78)$$

n is the refractive index, f_r is the radar frequency, and f_p is the plasma frequency. When the radar waves propagate through the ionosphere, their path bends due to the variation in reaction index caused by changes in electron density. This bending phenomenon is known as refraction. As the radar waves encounter regions of different electron densities, their speed and direction change, resulting in the bending of their path. This bending allows SuperDARN radar systems to observe ionospheric phenomena from below the horizon.

10.1.2 Typical radio wave ray path between the radar and the region of ionospheric scatter

Explain what is a typical radio wave ray path between the radar and the region of ionospheric scatter. Draw a diagram to illustrate this. Hint: what are ion mobilities in different directions with respect the geomagnetic field, and how does this affect formation of ionospheric irregularities.

The typical radio wave ray path between the radar and the region of ionospheric scatter involves several important considerations, including the geomagnetic field, ionospheric electron gradients, and the presence of ionospheric irregularities.

The Earth's geomagnetic field plays a crucial role in guiding the motion of charged particles in the ionosphere. The ion mobilities, the ability of ions to move in response to an electric field, vary depending on the direction with respect to the geomagnetic field. In regions where the geomagnetic field lines are aligned with the vertical direction, the ion mobility is typically higher. However, in regions where the geomagnetic field lines are perpendicular to the vertical direction, the ion mobility is lower.

The ionosphere exhibits gradients in electron density with altitude. The gradients can bend radio waves via refraction, causing the waves to follow a curved path. When radio waves encounter regions of higher electron density, they experience a decrease in velocity and bend toward the denser regions of higher electron density. Vice-versa, when they encounter region of lower electron density, they experience an increase in velocity and bend away from the denser regions.

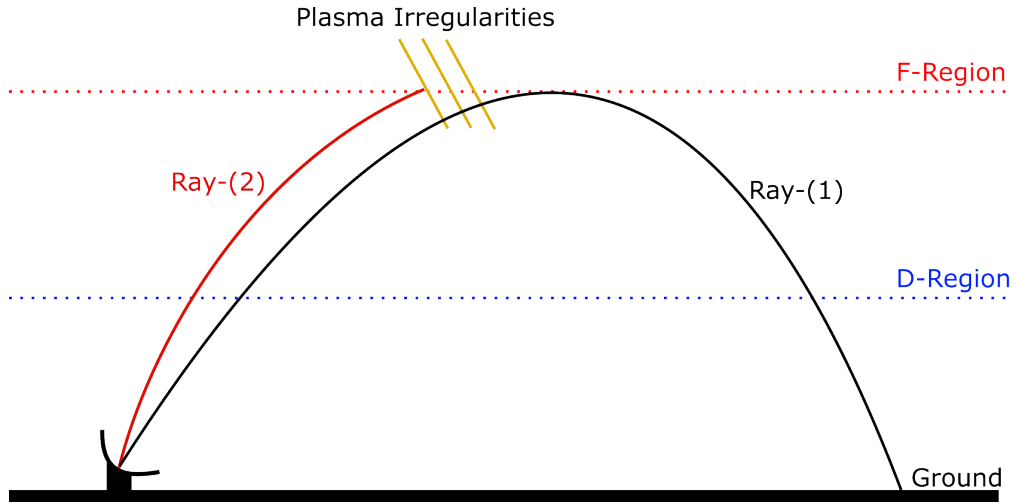


Figure 39: Illustration of radio wave ray path between the radar and the region of ionospheric scatter. (Trym Varland, 2024)

10.1.3 radar Bragg wave vector, scattered signal

What is the angle between the magnetic field and the radar Bragg wave vector for most of the contribution to the scattered signal? Why is this the case?

The angle between the magnetic field and the radar Bragg wave vector for most of the contribution to scattered signal is typically around 90 degrees or perpendicular. This orientation occurs because the radar Bragg vector is generally aligned with the direction of the incident radar beam, while the magnetic field is typically perpendicular to the radar beam in many cases. This perpendicular orientation maximizes the efficiency of the scattering process, resulting in a stronger scattered signal. It occurs due to the interaction between the electromagnetic wave and the charged particles in the ionosphere of the magnetosphere, where the magnetic field provides the necessary conditions for the scattering mechanism to occur effectively.

10.1.4 Information from the Doppler shift of F-region

What information does the Doppler shift of F-region ionospheric radar echoes measured by SuperDARN provide?

The Doppler shift of F-region ionospheric radar echoes measured by SuperDARN provides information about the movement and dynamics of charged particles in the Earth's ionosphere. Specifically, it helps determine the velocity of plasma flows along the radar line of sight. When these radars transmit radio waves into the ionosphere, these waves scatter off free electrons, creating echoes. The Doppler shift in the frequency of these echoes is caused by the motion of the scattering electrons relative to the radar. Which contains information about the velocity and direction of plasma convection in the ionosphere.

10.2 range-time diagram, different time lags of the autocorrelation function, multi-pulse scheme

The SuperDARN radar measures the averaged autocorrelation function of the scatter using a multi-pulse scheme. The Fourier transform of the autocorrelation function of radar scatter is the Doppler spectrum of the scattered signal. Draw a range-time diagram and explain how different time lags of the autocorrelation function are measured using the multi-pulse scheme.

Different time lags of the autocorrelation function were measured using the multi-pulse scheme. 1. The SuperDARN radar system transmits a series of radar pulses into the ionosphere. These pulses are transmitted at regular intervals. 2. As the radar pulses propagate through the ionosphere, they encounter free electrons. These electrons scatter the radar pulses, causing them to reflect back towards the radar receiver. 3. The radar receiver detected the echoes returning from the ionosphere. The received signals are then correlated with each other to compute the autocorrelation function. 4. The autocorrelation function is computed for various time lags, representing different delays between the transmitted and received radar pulses. The multi-pulse scheme involves using multiple pulses to obtain a more accurate estimation of the autocorrelation function. By averaging the autocorrelation function over multiple pulses, the radar system reduces noise and improves the reliability of the measurements. 5. The Fourier transform of the autocorrelation function yields the Doppler spectrum of the scattered signals. This spectrum represents the distribution of Doppler shifts of the radar echoes, providing information about the velocity and motion of plasma.

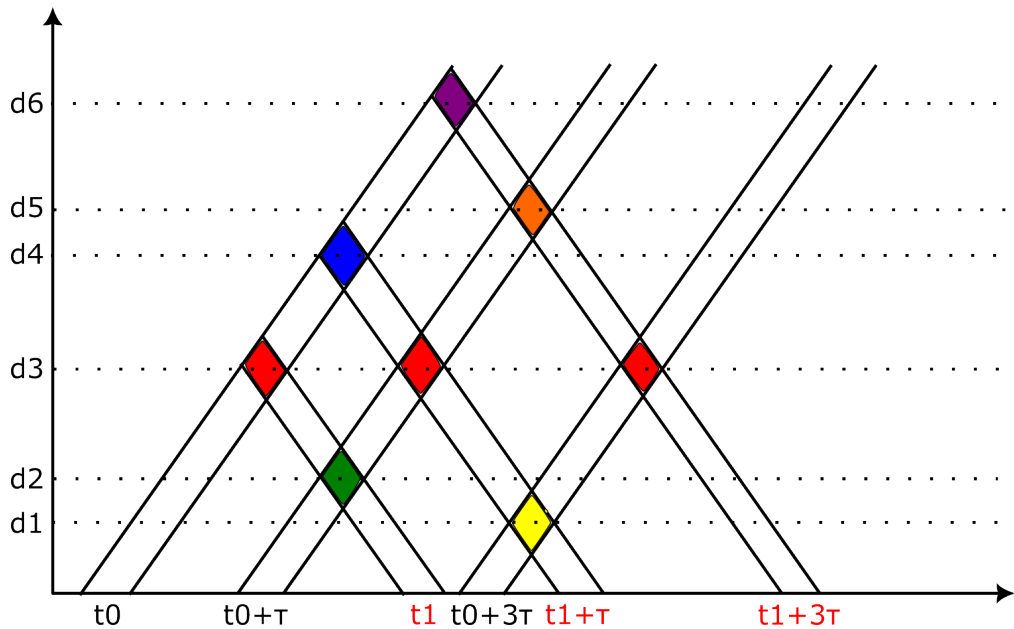


Figure 40: range-time diagram, (Trym Varland, 2024)

10.3 Northern Hemisphere polar cap convection patterns

Using the web site <https://superdarn.ca/convection-maps>, browser through the Northern Hemisphere polar cap convection patterns during the student campaign.

10.3.1 solar wind magnetic field, convection pattern

Make note of what the solar wind magnetic field is and compare it with the convection pattern. You can see the solar wind magnetic field on the top left corner of each convection mag plot.

We see from the plot that the solar wind magnetic field is about 3 to 4 nT, in the direction from -y to +z. We can see that the convection pattern have it's changes according to the incident direction of the solar wind magnetic field, hence why we that the convection pattern lays is in the opposite of the solar wind magnetic field direction and change accordingly.

10.3.2 ionospheric convection pattern, 2024-03-11T22:45

Find the Northern Hemisphere ionospheric convection pattern for the time period 2024-03-11T22:45. Indicate the location of the Harang discontinuity 16

The figure below shows the Northern Hemisphere ionospheric convection pattern, Where I have highlighted the location of the Harang discontinuity. We see the in the figure at the top on the left side, that we have the direction of the solar wind magnetic field is shifting from positive to negative. From this, we see in the ionospheric convection pattern there is a sudden change in direction of plasma flow.

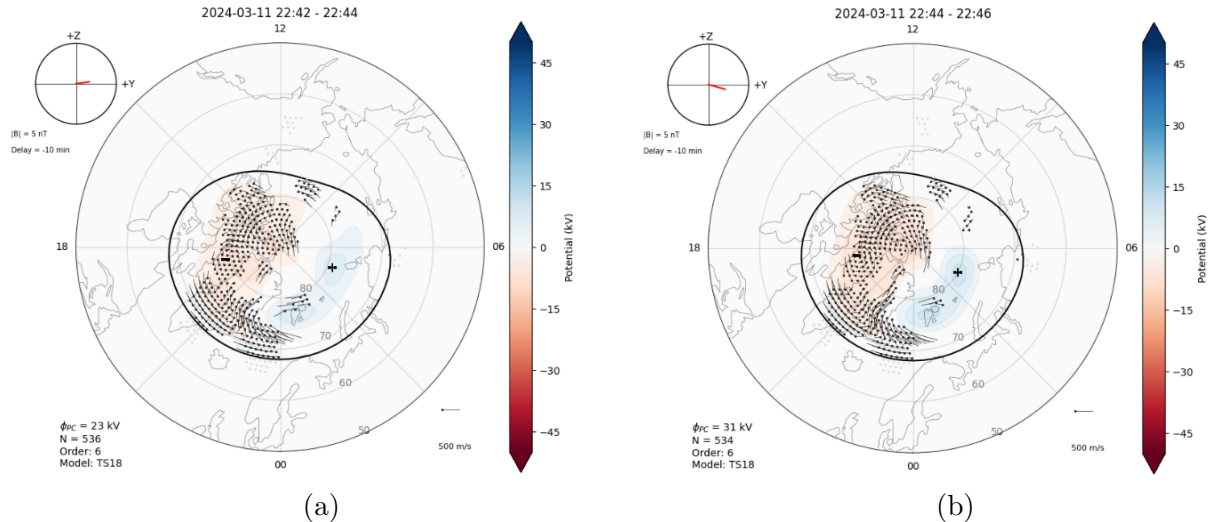


Figure 41: Northern Hemisphere ionospheric convection pattern, Harang discontinuity.

11 Appendix

References

- [1] C. G. Little and H. Leinbach. The riometer-a device for the continuous measurement of ionospheric absorption. *Proceedings of the IRE*, 47(2):315–320, Feb 1959.
- [2] Klaus Bibl and Bodo W. Reinisch. The universal digital ionosonde. *Radio Science*, 13(3):519–530, 1978.
- [3] V. A. Ivanov, V. I. Kurkin, V. E. Nosov, V. P. Uryadov, and V. V. Shumaev. Chirp Ionosonde and Its Application in the Ionospheric Research. *Radiophys. Quantum Electron.*, 46(11):821–851, November 2003.
- [4] Paul A. Wiegert. Hyperbolic meteors: Interstellar or generated locally via the gravitational slingshot effect? *Icarus*, 242:112–121, 2014.
- [5] GNSS Measurements Modelling - Navipedia, September 2023. [Online; accessed 10. Feb. 2024].
- [6] space.fmi.fi. KEV_091205.jpg (1260×570), April 2010. [Online; accessed 20. Mar. 2024].
- [7] Jeremy Kuzub. Keogram - Wikipedia, January 2024. [Online; accessed 20. Mar. 2024].